ELSEVIER

Mechanics of Materials 23 (1996) 71–102

MECHANICS OF MATERIALS

Localized deformation modes and non-Schmid effects in crystalline solids. Part I. Critical conditions of localization

Ming Dao, Robert J. Asaro *

Department of Applied Mechanics and Engineering Sciences, University of California, San Diego, Mail Code 0411, La Jolla, CA 92093, USA

Received 25 January 1995; revised version received 23 February 1996

Abstract

A general strain rate independent crystallographic slip theory which incorporates *non-Schmid effects*, is presented. This constitutive law is a rate independent isothermal idealization of the theory developed by Dao and Asaro (1993). The non-Schmid factors are estimated for Ni_3Al as well as for some simple metals. A general method to study the bifurcation modes for the general three-dimensional multiple slip geometry is described. Three-dimensional bifurcation analyses for single slip mode as well as multiple slip mode are presented. With moderate non-Schmid effects, *coarse slip bands* (CSB) are found possible in single slip modes as well as multiple slip modes, where critical localization criteria may be satisfied with significant strain hardening. Non-symmetric multiple slip geometries are examined and the bifurcation results show that shear bands close to the *conjugate* slip system are often more favored. Non-Schmid effects, elastic anisotropy and stress state may have important influences on the critical localization conditions. A mechanism for the transition from coarse slip bands to *macroscopic shear bands* (MSB) is suggested. The predictions of the theory are compared with existing experimental observations and good agreement is obtained for both the coarse slip bands and macroscopic shear bands.

1. Introduction

It has been realized that the localization of plastic flow in ductile crystals is not only common but appears to be an entirely natural, inevitable outcome of finite deformation processes. This is true for single crystals and polycrystals of simple metals and alloys. This is, in addition, also the case for crystalline materials which have ordered crystalline structures.

The relation between deviations from the Schmid rule of a critical resolved shear stress and localization of plastic deformation in ductile single crystals was first studied by Asaro and Rice (1977). They recognized that whereas the Schmid rule — which states that yielding occurs on a slip system when the resolved shear stress alone on that system reaches a critical value — is often a good approximation for simple crystals, deviations from it are inevitable. Asaro and Rice (1977) listed a number of familiar physical mechanisms which cause such deviations and present a detailed model analysis of cross-slip in what could either have been a crystal of a

* Corresponding author.

PII S0167-6636(96)00012-9

simple fcc or bcc metal or a more complex crystal such as an ordered intermetallic compound. Based on this they formulated a very general rate-independent yield criterion and a flow theory, and used it to analyze the bifurcation of a uniform state of plastic flow into states characterized by highly nonuniform and localized modes. Their results showed that such modes were possible even during single slip when the strain hardening rates on the individual slip systems fell below critical values on the order of $h_{cr}/G \leq \mathcal{O}(\eta^2)$ where G is a representative elastic constant and η stands for any one of a number of parameters that measure the extent to which other components of stress affect yielding on a slip system as compared to its resolved shear stress. The analysis was among the first to indicate reasons that uniform plastic flow in crystals is inherently unstable and how localization of deformation may occur in materials of nominally uniform properties and which are positively strain hardening. Subsequent analyses (e.g., Asaro, 1979; Chang and Asaro, 1981; Peirce et al., 1982; Peirce et al., 1983; Harren and Asaro, 1989; Bassani, 1994) showed that multiple slip involving the simultaneous activity on more than one slip system leads to further destabilization of flow and produces modes that involve nonuniform lattice rotations and *geometrical softening*.

Significant departures from the Schmid rule have been reported in crystals containing the $L1_2$ structure; for example in Ni_3Al by Paidar, Pope and Vitek (PPV, 1984) and in Ni_3Ga and Co_3Ti by Takeuchi and Kuramoto (1973) and Takasugi and Izumi (1987). Paidar et al. (1984) have, in fact, constructed a model for initial yielding of Ni_3Al using a cross-slip pinning dislocation model that fits within the general framework including the cross-slip dislocation models developed by Asaro and Rice (1977). In what follows we make specific contact with the PPV model as well as with independent experiment data for stress state dependent yielding in Ni_3Al crystals; some estimation for non-Schmid factors in simple fcc and bcc crystals are given as well. Nemat-Nasser et al. (1981) extended Asaro's model (Asaro, 1979) with plastic volume expansion and pressure sensitivity, giving a general analysis of strain localization. Recently Qin and Bassani (1992a); Qin and Bassani (1992b), within a rate-independent framework, applied the non-associated flow theory to Ni_3Al single crystals. The yield criterion they used was effectively the same as in Asaro and Rice (1977); their analyses are consistent with the original findings. Most recently, Dao and Asaro (1993) developed a general rate dependent crystallographic slip theory incorporating non-Schmid effects; their numerical results showed that the onset and further development of single slip shear bands are quite different from those of multiple slip shear bands.

There are some previous studies in metal plasticity and a large body of work in rock and soil mechanics which seek to model pressure sensitive materials (non-associate flow rule), since Coulomb proposed his yield criterion over 200 years ago. Relevant to this work, as far as the constitutive formulation is concerned, are the works by Mandel (1947), Spencer (1964), Mehrabadi and Cowin (1978), Mehrabadi and Cowin (1980), and Christoffersen et al. (1981), who proposed models based on double slip taking into account the pressure sensitivity and in the latter works the plastic volume change. In geomechanics, as far as localization analysis is concerned, some early contributions are by Vardoulakis et al. (1978), Mehrabadi and Cowin (1980) and Nemat-Nasser (1983). A model is recently developed by Drucker and Li (1993) and Li and Drucker (1994) to explain the instability and bifurcation on the basis of a non-associated flow rule, which is different from the earlier approach, e.g., by Rudnicki and Rice (1975).

Although in simple metals, non-Schmid effects are usually small, non-Schmid factors as small as 0.04 (easily unnoticed in experimental verifications of the Schmid rule) can be the cause for localization at quite high hardening rates (see, e.g. Asaro and Rice (1977), Chang and Asaro (1981) and Dao and Asaro (1993); Dao and Asaro (1994)). In the present work, efforts are made to understand the formation of *coarse slip bands* (CSB) and the transition to *macroscopic shear bands* (MSB). In this regard, Chang and Asaro (1981) found that the critical conditions for the onset of CSB's are related to that of the single slip shear bands predicted by Asaro and Rice (1977), where the presence of small non-Schmid effects was believed to be the major factor. Dao and Asaro (1994), using large scale finite element calculations, confirmed that, indeed, the small non-Schmid effects can result in CSB's and, later on, trigger MSB's.

This article represents the first part of two describing non-Schmid effects and localized deformation in crystalline solids and shall be referred to as Part I. Here a rate independent version of a finite deformation slip

theory incorporating non-Schmid effects is presented and a general method is applied to study the critical conditions of localization. In the second article, referred to as Part II, a rate-dependent version of the finite deformation slip theory incorporating non-Schmid effects is introduced where large scale finite element calculations are carried out to study the deformation patterns and the development of localized deformation processes. Some preliminary results can be found in Dao and Asaro (1993); Dao and Asaro (1994).

In this paper, we present a general strain rate independent version of a finite deformation slip theory that specifically accounts for deviations from Schmid's rule. It is, in fact, a rate independent idealization of the model developed by Dao and Asaro (1993). A general method is presented to study the critical conditions of localization in three-dimensional geometry. Unlike previous studies where only two-dimensional slip geometry is used to study the localization for general multiple slip mode, the procedure given in this paper can account for three-dimensional multiple slip geometries, elastic anisotropy, and different stress states. The predictions of the critical conditions for localization are consistent with those existing experimental observations. A comprehensive analysis about the non-Schmid effects and the polycrystal behavior was done in another paper (Dao et al., 1996).

The plan of this paper is as follows: In the next section, we review experimental observations and interpretations of CSB's and MSB's to place our analyses in perspective; in Section 3 the constitutive theory is presented and, Section 3.2 introduces a general method to perform three-dimensional bifurcation analyses. Section 4.1 gives some estimated non-Schmid factors for Ni_3Al; in Section 4.2 some estimation of non-Schmid factors for simple metals are given. Three-dimensional bifurcation analyses for single slip mode and multiple slip mode are presented in Sections 5.1 and 5.2, respectively. A brief summary is given in Section 5.3. Discussions follow in Section 6.

1.1. Notations

Standard tensor notation is used throughout. Bold faced symbols are used to denote vectors and higher order tensors, the order of which will be clear in context. Products are indicated with dots, which denote summation over repeated Latin indices, and products containing no dots are dyadic products. Latin indices range from one to the number of spatial dimensions, and repeated Latin indices are always summed. Inverses, transposes, and transposed inverses are denoted with a superscripted -1, T and $-$T, respectively and superposed dots indicate differentiation with respect to time t. For example,

$$\boldsymbol{A}\cdot\boldsymbol{B}=A_{ik}B_{kj}\boldsymbol{b}_i\boldsymbol{b}_j;\quad \boldsymbol{A}\times\boldsymbol{B}=e_{ijk}A_jB_k\boldsymbol{b}_i;$$

$$\boldsymbol{A}{:}\boldsymbol{B}=A_{ij}B_{ji};\quad \boldsymbol{AB}=A_{ij}B_{kl}\boldsymbol{b}_i\boldsymbol{b}_j\boldsymbol{b}_k\boldsymbol{b}_l;$$

$$\boldsymbol{cd}=c_id_j\boldsymbol{b}_i\boldsymbol{b}_j;\quad \boldsymbol{B}\cdot\boldsymbol{c}=B_{ij}c_j\boldsymbol{b}_i;$$

$$\boldsymbol{H}{:}\boldsymbol{A}=H_{ijkl}A_{lk}\boldsymbol{b}_i\boldsymbol{b}_j;\quad \frac{\partial\boldsymbol{c}}{\partial\boldsymbol{d}}=\frac{\partial c_i}{\partial d_j}\boldsymbol{b}_i\boldsymbol{b}_j;$$

$$\dot{\boldsymbol{B}}=\frac{\partial B_{ij}}{\partial t}\boldsymbol{b}_i\boldsymbol{b}_j,$$

where e_{ijk} is the permutation symbol. The basis, $\boldsymbol{b}_i$, is Cartesian and independent of time. Greek indices are used to identify slip systems and range from one to N = the number of slip systems. Summation over repeated nonparenthetical Greek indices is implied while repeated parenthetical Greek indices are not summed, e.g., $\boldsymbol{c}_\alpha\boldsymbol{d}_\alpha$ means $\boldsymbol{c}_1\boldsymbol{d}_1+\boldsymbol{c}_2\boldsymbol{d}_2+\ldots+\boldsymbol{c}_N\boldsymbol{d}_N$ and $\boldsymbol{c}_\alpha\boldsymbol{d}_{(\alpha)}$ means either $\boldsymbol{c}_1\boldsymbol{d}_1$, $\boldsymbol{c}_2\boldsymbol{d}_2$, ..., or $\boldsymbol{c}_N\boldsymbol{d}_N$.

2. Perspectives on coarse slip bands and macroscopic shear bands

Three localized deformation modes in single crystals are studied here: (i) diffuse necking, (ii) coarse slip bands and (iii) macroscopic shear bands. These three modes are often observed during large deformation of a single crystal, and are often observed simultaneously on the same sample crystal during deformation.

2.1. CSB's and MSB's in simple metals

As an example, precipitation hardened alloys containing GP-I and GP-II zones form an interesting class of material which displays intense shear bands leading to fracture. Elam (1927) performed early experiments on Al–Zn single crystals, Beevers and Honeycombe (1962) on Al–Cu, Price and Kelly (1964) on Al–Cu, Al–Zn, Al–Ag and Cu–Be single crystals, and Chang and Asaro (1981) on Al–Cu single crystals. Chang and Asaro (1981) and Chang (1979) have done systematic experiments on Al–2.8wt%Cu single crystals (fcc) in simple tension and compression; Harren et al. (1988) performed tests in plane strain compression on Al–2.8wt%Cu single crystals. There are characteristic observations on the formation of coarse slip bands and macroscopic shear bands which are important to outline.

Fig. 1 shows CSB and MSB formation in a GP-II Al–2.8wt%Cu single crystal. The crystal is oriented such that slip begins on the *primary* slip system where after the lattice rotations that occur induce slip on a second system, the *conjugate* slip system. The CSB's formed on the primary slip system first, then became clustered, and finally within the cluster of CSB's, an MSB formed. The orientation difference between CSB's and the MSB is one characteristic observation. Fig. 2 shows CSB and MSB formation in another GP-II Al–2.8wt%Cu single crystal. It was observed that CSB's formed first on the primary slip plane and then a MSB formed on the conjugate slip plane. Additional observations by Chang and Asaro (1981) and Chang (1979) show that, in addition to the two cases in Figs. 1 and 2, CSB's may form first on planes close to the conjugate slip plane and subsequently MSB's may form on planes near the primary or conjugate slip plane. Fig. 3 shows CSB and MSB formation in an Al–2.8wt%Cu single crystal; CSB's formed first on the conjugate slip plane, the CSB's then clustered and finally a MSB formed on the conjugate slip plane within the CSB cluster. Fig. 4 shows a Al–2.8wt%Cu single crystal under compression, the loading axis was oriented for symmetric slip on both primary and conjugate slip planes. The CSB pattern was clearly shown on both primary and conjugate slip

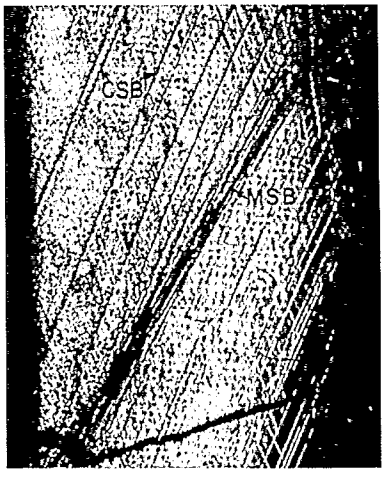

Fig. 1. CSB and MSB formation in a GP-II Al–2.8wt%Cu single crystal. The CSB's formed on the primary slip system at first, then became clustered and finally within the cluster of CSB's formed an MSB. Noting that the orientation difference between CSB's and the MSB. (Photo taken from Chang and Asaro, 1981.)

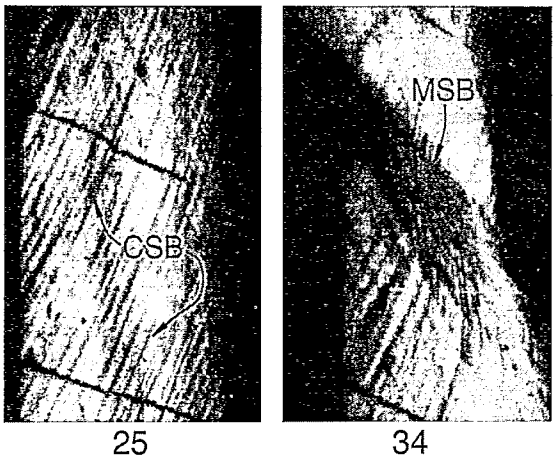

Fig. 2. CSB and MSB formation in a GP-II Al–2.8wt%Cu single crystal. CSB's formed first on the primary slip plane (frame 25) and then a MSB formed on the conjugate slip plane (frame 34). (Photo taken from Chang, 1979.)

planes. Localized deformation modes of the CSB or MSB type are observed in bcc crystals as well, i.e. Spitzig (1981) and Dève et al. (1988) have reported on the shear band formation in Fe–Ti–Mn single crystals (bcc) and Reid et al. (1966) in Nb single crystals.

2.2. Intermetallic compounds

CSB patterns have been observed in ordered intermetallic compounds such as Ni_3Ga ($L1_2$) (Takeuchi and Kuramoto, 1973), TiAl ($L1_0$) (Kawabata et al., 1985) and Ti_3Al ($D0_{19}$) (Minonishi, 1991). Fig. 5 shows examples of compression tests along a fixed orientation at three different temperatures for Ni_3Ga. CSB's are clearly observed at the low temperature (77 K) and as well as at the higher temperature (993 K); the spacing between coarse slip bands are much smaller at 993 K than at 77 K. At the intermediate temperature, deformation looks very much uniform. From our analyses, it appears that at the intermediate temperature (458 K) the hardening rate is too high to meet the critical conditions for localization, although the non-Schmid effects are

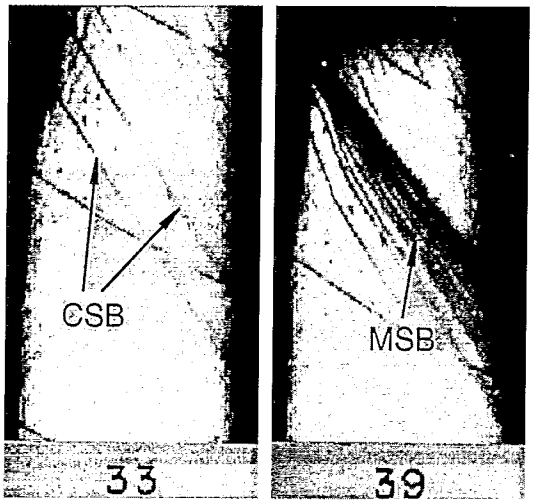

Fig. 3. CSB and MSB formation in an Al–Cu single crystal. CSB's formed first on the conjugate slip plane (frame 33), the CSB's then clustered and finally a MSB formed on the conjugate slip plane within the CSB cluster (frame 39). (Photo taken from Chang, 1979.)

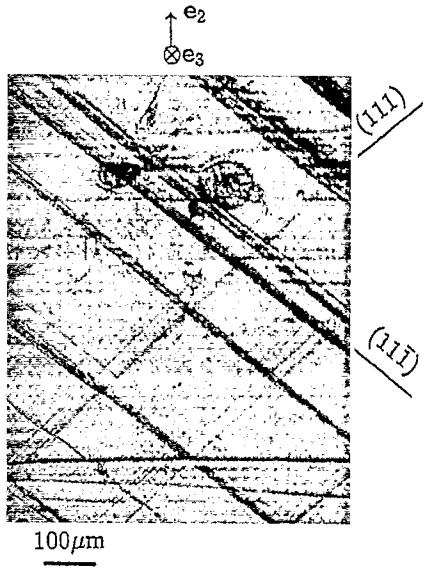

Fig. 4. An Al–2.8wt%Cu single crystal under compression, the loading axis was oriented for symmetric slip on both primary and conjugate slip planes. The CSB pattern was clearly shown on both primary and conjugate slip planes. (Photo taken from Harren et al., 1988.)

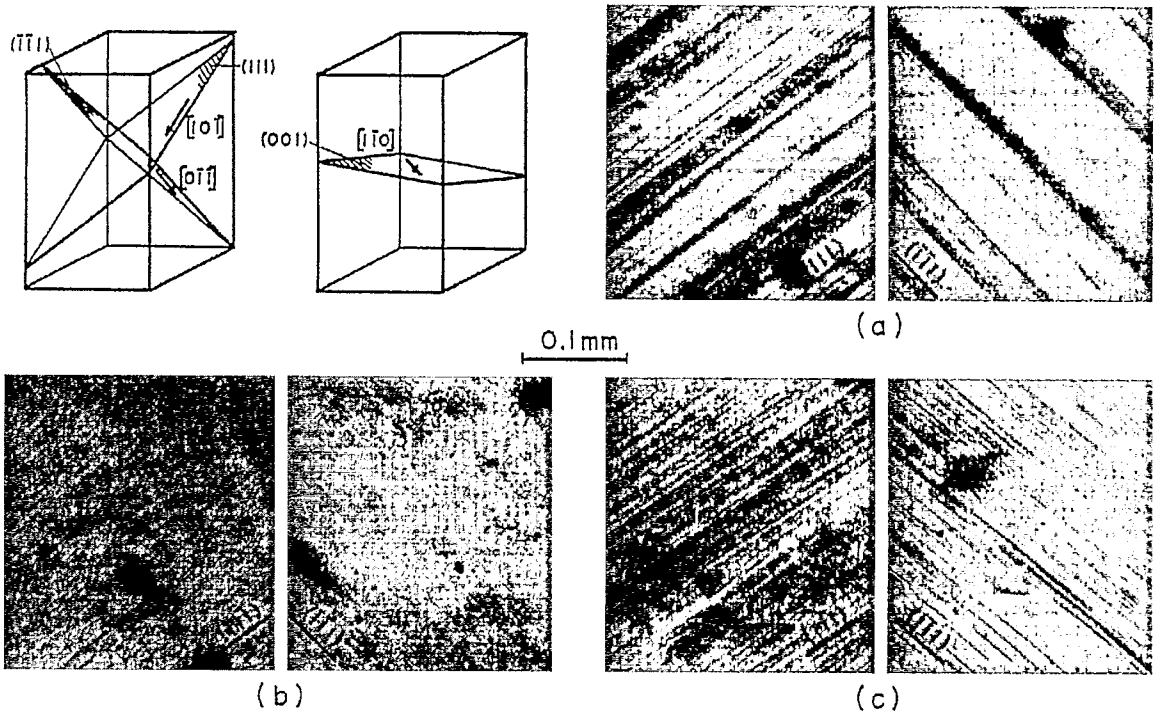

Fig. 5. Compression tests along a fixed orientation at three different temperatures for Ni_3Ga. (Photo taken from Takeuchi and Kuramoto, 1973.) We can see clearly CSB's at low temperature (77 K) and high temperature (993 K), the spacing between coarse slip bands are much shorter at 993 K than that of 77 K. In the intermediate temperature test, deformation looks very much uniform.

the strongest around the anomalous temperature. Heredia and Pope (1989) studied Ni_3Al ($L1_2$) single crystals in tension. They found that the crystals often fracture on {111}-type shear planes. Such abruptly occurring localized plastic flow has been reported in crystals of other ordered intermetallic compounds such as NiAl (Wasilewski et al., 1967) as well as in TiAl alloys containing duplex γ/α_2 microstructures (Inui et al., 1992). What appears to be common to these materials is that they display stable and, often high, rates of strain hardening, yet fail via highly concentrated shearing.

2.3. Summary of experimental observations on CSB's and MSB's

To summarize the observations from previous experiments, we conclude that

(1) CSB's often appear before any obvious necking and load drop; MSB's usually form after necking and after the load drop.

(2) In single crystals originally oriented for single slip, CSB's can initiate on both primary and conjugate slip systems; MSB's can initiate on both primary and conjugate slip systems as well.

(3) CSB's are closely aligned with the active slip planes; MSB's are typically several degrees (5°–10°) misoriented with respect to the active slip planes. MSB's can initiate at planes closely aligned with the active slip planes, but when the deformation gets larger they usually rotate further away from the active slip planes.

(4) CSB's may initiate under single slip modes as well as multiple slip modes; MSB's are believed to initiate under multiple slip mode (Asaro, 1979; Peirce et al., 1982; Peirce et al., 1983; Dao and Asaro, 1993).

(5) Clustering of CSB's appears to be part of the formation of MSB's.

(6) In intermetallic compounds, CSB's are often found. These materials usually have stable and, often high, rates of strain hardening yet fail via highly concentrated shearing. Significant deviations from Schmid's Law are observed in Ni_3Ga (Takeuchi and Kuramoto, 1973) and Ni_3Al (Paidar et al., 1984).

MSB's have been studied extensively, i.e. Asaro (1979), Peirce et al. (1982); Peirce et al. (1983); Dao and Asaro (1993); Dao and Asaro (1994). *Geometrical softening*, caused by the non-uniform lattice rotations within the shear bands, was found to be the major factor in triggering MSB's. Dao and Asaro (1993); Dao and Asaro (1994) found that non-Schmid effects may significantly affect the critical conditions of localization. To explain the formation of CSB's, Price and Kelly (1964) had suggested that CSB's may develop at quite high hardening rates as they do not tend to persist at the same location but, instead, tend to be coarsely spread along the active gage length of the crystals. Chang and Asaro (1981) found that the critical conditions for the onset of CSB's are related to that of the single slip shear bands predicted by Asaro and Rice (1977), where the presence of small non-Schmid effects was believed to be the major factor. Most recently, in a preliminary report, Dao and Asaro (1994) confirmed that small non-Schmid effects combined with high hardening rates (but lower than the critical hardening rate of localization in single slip) can result in CSB's, and saturating (positive) hardening rates with deformation can result in clustering of CSB's and initiation of MSB's. There are, however, outstanding questions that need further explanation, e.g.: (i) why CSB's often form first on conjugate slip system, and what are the critical conditions; (ii) why MSB's often form first on the conjugate slip system, and what are the critical conditions; (iii) why and under what conditions do CSB's form under multiple slip modes; (iv) how do we categorize CSB's and MSB's with respect to single slip shear bands and multiple slip shear bands. To answer such questions along with studying the experimentally observed phenomena listed above, we have extended our focus to three-dimensional non-symmetric slip geometry, incorporating non-Schmid effects in single slip as well as multiple slip modes.

3. The theory and numerical considerations

3.1. The rate-independent constitutive law

The rate-independent constitutive law can be written in a form developed by Hill and Rice (1972); Asaro and Rice (1977); Asaro (1979) and Hill and Havner (1982), which is based on the pioneering work of Taylor (1938).

What we add here is the non-Schmid effects for the multiple slip mode. It is the rate-independent and isothermal idealization of the rate-dependent version of Dao and Asaro (1993). Recently Qin and Bassani (1992a); Qin and Bassani (1992b), within the rate-independent framework, developed a slightly different form, where only pure shear stresses are taken into consideration as sources of non-Schmid effects.

Assume there are $\alpha = 1, 2, \ldots, N$ slip systems active, where $N = 1$ stands for single slip, $N = 2$ stands for double slip, $N = 3$ stands for triple slip, ... Slip system α is defined by orthogonal unit vectors s_α, m_α and z_α, where s_α is the current slip direction, m_α is normal to the slip plane and z_α is normal to both s_α and m_α. The total deformation rate $\boldsymbol{D}$ and spin rate $\boldsymbol{\Omega}$ are composed by two parts. The first part is the plastic part, where material deforms by shearing along the various slip systems of the crystal; the plastic deformation rate $\boldsymbol{D}^P$ and the plastic spin rate $\boldsymbol{\Omega}^P$ are given by

$$\boldsymbol{D}^P = \boldsymbol{P}_\alpha \dot{\gamma}_\alpha \quad \text{and} \quad \boldsymbol{\Omega}^P = \boldsymbol{W}_\alpha \dot{\gamma}_\alpha, \tag{3.1}$$

respectively, where $\dot{\gamma}_\alpha$ is the shearing rate of the α slip system, and

$$\boldsymbol{P}_\alpha = \tfrac{1}{2}(\boldsymbol{s}_\alpha \boldsymbol{m}_\alpha + \boldsymbol{m}_\alpha \boldsymbol{s}_\alpha), \tag{3.2a}$$

and

$$\boldsymbol{W}_\alpha = \tfrac{1}{2}(\boldsymbol{s}_\alpha \boldsymbol{m}_\alpha - \boldsymbol{m}_\alpha \boldsymbol{s}_\alpha). \tag{3.2b}$$

The second part is the elastic plus lattice rotation part, where material deforms by elastic deformation and the lattice rotations; this part of deformation rate and spin rate are denoted by $\boldsymbol{D}^*$ and $\boldsymbol{\Omega}^*$, respectively. Thus we can add the two parts together to obtain

$$\boldsymbol{D} = \boldsymbol{D}^* + \boldsymbol{P}_\alpha \dot{\gamma}_\alpha, \tag{3.3a}$$

and

$$\boldsymbol{\Omega} = \boldsymbol{\Omega}^* + \boldsymbol{W}_\alpha \dot{\gamma}_\alpha. \tag{3.3b}$$

Take the lattice deformation to be elastic and unaffected by the plastic slips, let $\boldsymbol{L}$ to be the elastic moduli phrased relatively to lattice directions, then

$$\overset{\triangledown}{\boldsymbol{\sigma}}{}^* + \boldsymbol{\sigma}\,\mathrm{tr}(\boldsymbol{D}^*) = \boldsymbol{L}{:}\boldsymbol{D}^*, \tag{3.4}$$

where

$$\overset{\triangledown}{\boldsymbol{\sigma}}{}^* = \dot{\boldsymbol{\sigma}} - \boldsymbol{\Omega}^* \cdot \boldsymbol{\sigma} + \boldsymbol{\sigma} \cdot \boldsymbol{\Omega}^*, \tag{3.5}$$

where $\dot{\boldsymbol{\sigma}}$ is the ordinary time rate of Cauchy stress, $\boldsymbol{\sigma}$, following the material element and Cartesian components of

$$\overset{\triangledown}{\boldsymbol{\sigma}}{}^*$$

are the ordinary time rates of the components of $\boldsymbol{\sigma}$ on axes that rotate rigidly at the lattice spin rate $\boldsymbol{\Omega}^*$. To study material deformation, we also need a stress rate whose components are formed on axes that spin with the material as given by

$$\overset{\triangledown}{\boldsymbol{\sigma}} = \dot{\boldsymbol{\sigma}} - \boldsymbol{\Omega} \cdot \boldsymbol{\sigma} + \boldsymbol{\sigma} \cdot \boldsymbol{\Omega}. \tag{3.6}$$

The two rates,

$$\overset{\triangledown}{\boldsymbol{\sigma}}{}^* \text{ and } \overset{\triangledown}{\boldsymbol{\sigma}},$$

are related by

$$\overset{\triangledown}{\boldsymbol{\sigma}} - \overset{\triangledown}{\boldsymbol{\sigma}}^{*} = (\boldsymbol{\sigma}\cdot W_\alpha - W_\alpha\cdot\boldsymbol{\sigma})\dot{\gamma}_\alpha. \tag{3.7}$$

Expressing $\boldsymbol{D}^{*}$ and $\boldsymbol{\Omega}^{*}$ in terms of $\boldsymbol{D}$ and $\boldsymbol{\Omega}$ using Eq. (3.3), Eq. (3.4) becomes

$$\overset{\triangledown}{\boldsymbol{\sigma}} + \boldsymbol{\sigma}\,\mathrm{tr}(\boldsymbol{D}) = \boldsymbol{L}:\left\{\boldsymbol{D} - \hat{\boldsymbol{P}}_\alpha\dot{\gamma}_\alpha\right\}, \tag{3.8}$$

with

$$\hat{\boldsymbol{P}}_\alpha = \boldsymbol{P}_\alpha + \boldsymbol{L}^{-1}:(W_\alpha\cdot\boldsymbol{\sigma} - \boldsymbol{\sigma}\cdot W_\alpha). \tag{3.9}$$

Following Dao and Asaro (1993), the general yield criterion is given as

$$\tau_\alpha + \boldsymbol{\eta}_\alpha:\boldsymbol{\sigma} = \boldsymbol{m}_\alpha\cdot\boldsymbol{\sigma}\cdot\boldsymbol{s}_\alpha + \boldsymbol{\eta}_\alpha:\boldsymbol{\sigma} = g_\alpha, \tag{3.10}$$

where τ_α is the current value of the resolved shear stress, g_α is the current resistance, and $\boldsymbol{\eta}_\alpha$ is the tensor of non-Schmid effects for slip system α which, when aligned with $\boldsymbol{s}_\alpha$, $\boldsymbol{m}_\alpha$ and $\boldsymbol{z}_\alpha$, takes the simple form

$$\boldsymbol{\eta} = \begin{pmatrix} \eta_{ss} & 0 & \eta_{sz} \\ 0 & \eta_{mm} & \eta_{mz} \\ \eta_{sz} & \eta_{mz} & \eta_{zz} \end{pmatrix}. \tag{3.11}$$

If the slip system α is to remain active, taking derivatives of both sides of Eq. (3.10) with respect to time t, we must have

$$\frac{\mathrm{d}(\boldsymbol{m}_\alpha\cdot\boldsymbol{\sigma}\cdot\boldsymbol{s}_\alpha + \boldsymbol{\eta}_\alpha:\boldsymbol{\sigma})}{\mathrm{d}t} = h_{\alpha\beta}\dot{\gamma}_\beta, \tag{3.12}$$

where $h_{\alpha\beta}$ is a hardening matrix, the off diagonal elements of which represent latent hardening. The explicit form of the left-hand side of Eq. (3.12) depends on how $\dot{\boldsymbol{s}}_\alpha$ and $\dot{\boldsymbol{m}}_\alpha$ are defined. Asaro and Rice (1977) discussed various possibilities which differ in how lattice elasticity is accounted for, and practically same results were obtained. For the present, we will assume that $\boldsymbol{s}_\alpha$ and $\boldsymbol{m}_\alpha$ remain othogonal unit vectors and simply rotate rigidly at the lattice spin rate $\boldsymbol{\Omega}^{*}$. Thus, in view of Eq. (3.11), after some rearrangements, we obtain

$$\frac{\mathrm{d}(\boldsymbol{m}_\alpha\cdot\boldsymbol{\sigma}\cdot\boldsymbol{s}_\alpha + \boldsymbol{\eta}_\alpha:\boldsymbol{\sigma})}{\mathrm{d}t} = \boldsymbol{Q}_\alpha:\overset{\triangledown}{\boldsymbol{\sigma}}^{*}, \tag{3.13a}$$

with

$$\boldsymbol{Q}_\alpha = \boldsymbol{P}_\alpha + \boldsymbol{T}^\alpha\cdot\boldsymbol{\eta}\cdot\boldsymbol{T}^{\alpha\mathrm{T}}, \tag{3.13b}$$

where $\boldsymbol{T}^\alpha$ is the transformation tensor between lab axes $\boldsymbol{a}_i$ and the α slip system $\boldsymbol{s}_\alpha$, $\boldsymbol{m}_\alpha$, $\boldsymbol{z}_\alpha$, i.e. if $\boldsymbol{e}_1^\alpha = \boldsymbol{s}_\alpha$, $\boldsymbol{e}_2^\alpha = \boldsymbol{m}_\alpha$, $\boldsymbol{e}_3^\alpha = \boldsymbol{z}_\alpha$, then $\boldsymbol{T}_{ij}^\alpha = \boldsymbol{a}_i\cdot\boldsymbol{e}_j^\alpha$. From Eqs. (3.12) and (3.13), a general flow rule, incorporating non-Schmid effects, is simply given as

$$\left(\boldsymbol{P}_\alpha + \boldsymbol{T}^\alpha\cdot\boldsymbol{\eta}\cdot\boldsymbol{T}^{\alpha\mathrm{T}}\right):\overset{\triangledown}{\boldsymbol{\sigma}}^{*} = \boldsymbol{Q}_\alpha:\overset{\triangledown}{\boldsymbol{\sigma}}^{*} = h_{\alpha\beta}\dot{\gamma}_\beta. \tag{3.14}$$

Replacing $\boldsymbol{D}^{*}$ and $\boldsymbol{\Omega}^{*}$ with $\boldsymbol{D}$ and $\boldsymbol{\Omega}$ from Eq. (3.3) and using Eq. (3.4) to evaluate

$$\overset{\triangledown}{\boldsymbol{\sigma}}^{*},$$

Eq. (3.14) becomes

$$\boldsymbol{L}:\left\{\boldsymbol{D} - \boldsymbol{P}_\beta\dot{\gamma}_\beta\right\}:\boldsymbol{Q}_\alpha = h_{\alpha\beta}\dot{\gamma}_\beta. \tag{3.15}$$

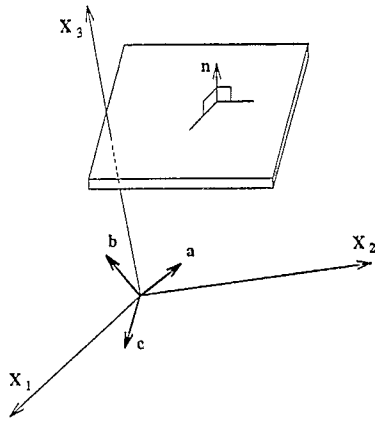

Fig. 6. Cartesian coordinates and reference crystal axes a, b and c, where the right hand triad a, b and c are some specific crystallographic directions of the single crystal. Surface of localization is shown with unit normal n, having components n_1, n_2 and n_3.

Inverting Eq. (3.15) we have

$$\dot{\gamma}_\alpha = N^{-1}_{\alpha\beta} \boldsymbol{Q}_\beta : \boldsymbol{L} : \boldsymbol{D}, \tag{3.16a}$$

where

$$N_{\alpha\beta} = h_{\alpha\beta} + \boldsymbol{Q}_\alpha : \boldsymbol{L} : \boldsymbol{P}_\beta. \tag{3.16b}$$

Finally, with Eq. (3.16), Eq. (3.8) becomes

$$\overset{\triangledown}{\boldsymbol{\sigma}} + \boldsymbol{\sigma}\,\mathrm{tr}(\boldsymbol{D}) = \boldsymbol{L} : \boldsymbol{D} - \left(\boldsymbol{L} : \hat{\boldsymbol{P}}_\alpha\right) N^{-1}_{\alpha\beta} \left(\boldsymbol{Q}_\beta : \boldsymbol{L} : \boldsymbol{D}\right). \tag{3.17}$$

3.2. A general method for three-dimensional bifurcation analyses

For materials described by idealized rate-independent constitutive laws Hill (1962) has given a general theory of bifurcation of a homogeneous elastic-plastic flow field into bands of localized deformation. For this to occur there is first the kinematical restriction that for localization in a thin planar band with unit normal $\boldsymbol{n}$ (see Fig. 6) the velocity gradient field inside the band $\partial \boldsymbol{v}/\partial \boldsymbol{x}$ can differ from that outside, $\partial \boldsymbol{v}^0/\partial \boldsymbol{x}$, as

$$\frac{\partial \boldsymbol{v}}{\partial \boldsymbol{x}} - \frac{\partial \boldsymbol{v}^0}{\partial \boldsymbol{x}} = \boldsymbol{g}\boldsymbol{n}. \tag{3.18}$$

In addition, there is the continuing equilibrium requirement that

$$\boldsymbol{n} \cdot \dot{\boldsymbol{\sigma}} - \boldsymbol{n} \cdot \dot{\boldsymbol{\sigma}}^0 = \boldsymbol{0} \tag{3.19}$$

at incipient localization where $\dot{\boldsymbol{\sigma}}$ is the stress rate inside the band and $\dot{\boldsymbol{\sigma}}^0$ that outside.

Constitutive law Eq. (3.17) along with the conditions for localization (Eqs. (3.18) and (3.19)) can be solved to get critical conditions for the onset of localization. We first rewrite Eq. (3.17) to be

$$\dot{\boldsymbol{\sigma}} = \left\{\boldsymbol{L} - \left(\boldsymbol{L} : \hat{\boldsymbol{P}}_\alpha\right) N^{-1}_{\alpha\beta} \left(\boldsymbol{Q}_\beta : \boldsymbol{L}\right)\right\} : \boldsymbol{D} + \boldsymbol{\Omega} \cdot \boldsymbol{\sigma} - \boldsymbol{\sigma} \cdot \boldsymbol{\Omega} - \boldsymbol{\sigma}\,\mathrm{tr}(\boldsymbol{D}). \tag{3.20}$$

and recognizing that $\boldsymbol{D}$ and $\boldsymbol{\Omega}$ can be expressed in terms of the velocity gradient. With Eq. (3.18) in mind, we have

$$\boldsymbol{D} - \boldsymbol{D}^0 = \tfrac{1}{2}(\boldsymbol{g}\boldsymbol{n} + \boldsymbol{n}\boldsymbol{g}), \tag{3.21a}$$

and

$$\boldsymbol{\Omega} - \boldsymbol{\Omega}^0 = \tfrac{1}{2}(\boldsymbol{g}\boldsymbol{n} - \boldsymbol{n}\boldsymbol{g}), \tag{3.21b}$$

where $\boldsymbol{D}$ and $\boldsymbol{\Omega}$ are measured inside the shear band and $\boldsymbol{D}^0$ and $\boldsymbol{\Omega}^0$ are that outside. Multiplying Eq. (3.20) from the left with $\boldsymbol{n}$ and using Eqs. (3.19) and (3.21), we obtain

$$\left\{\boldsymbol{n}\cdot\boldsymbol{L}\cdot\boldsymbol{n} - \left(\boldsymbol{n}\cdot\boldsymbol{L}:\hat{\boldsymbol{P}}_\alpha\right)N^{-1}_{\alpha\beta}\left(\boldsymbol{Q}_\beta:\boldsymbol{L}\cdot\boldsymbol{n}\right)\right\}\cdot\boldsymbol{g} + \boldsymbol{A}\cdot\boldsymbol{g} = \boldsymbol{0}, \tag{3.22a}$$

where

$$\boldsymbol{A} = \tfrac{1}{2}\{(\boldsymbol{n}\cdot\boldsymbol{\sigma}\cdot\boldsymbol{n})\boldsymbol{I}^{(2)} - \boldsymbol{\sigma} - (\boldsymbol{n}\cdot\boldsymbol{\sigma})\boldsymbol{n} - \boldsymbol{n}(\boldsymbol{\sigma}\cdot\boldsymbol{n})\}, \tag{3.22b}$$

and $\boldsymbol{I}^{(2)}$ is the second order identity tensor with $I^{(2)}_{ij} = \delta_{ij}$. Let

$$\boldsymbol{M} = \boldsymbol{n}\cdot\boldsymbol{L}\cdot\boldsymbol{n} - \left(\boldsymbol{n}\cdot\boldsymbol{L}:\hat{\boldsymbol{P}}_\alpha\right)N^{-1}_{\alpha\beta}\left(\boldsymbol{Q}_\beta:\boldsymbol{L}\cdot\boldsymbol{n}\right) + \boldsymbol{A}, \tag{3.23}$$

then Eq. (3.22a) becomes

$$\boldsymbol{M}\cdot\boldsymbol{g} = \boldsymbol{0}. \tag{3.24}$$

Now we can solve for the critical conditions of localization using

$$\det\{\boldsymbol{M}\} = 0. \tag{3.25}$$

Only in some special cases, a close form solution can be obtained for Eq. (3.25). To study more general cases, like non-symmetric slip geometry, three-dimensional multiple slip modes and anisotropic crystal elasticity, we will use a numerical method to solve for Eq. (3.25). In this study, a simple bisection method is used to find solutions.

4. Estimation of the non-Schmid factors

4.1. Estimation of non-Schmid factors in Ni_3Al

Dao and Asaro (1993) have estimated the non-Schmid factors for Ni_3Al at several different temperatures (see Table 1).

Table 1
Non-Schmid factors for Ni_3Al at several temperatures

Temperature	Stress state	η_{ss}	η_{mm}	η_{zz}	η_{mz}	η_{sz}
$\theta = 293$ K	$\tau_{sm} > 0, \tau_{cb} > 0$	0	0.008	−0.008	0.008	−0.015
	$\tau_{sm} < 0, \tau_{cb} < 0$	0	−0.008	0.008	−0.008	−0.015
	$\tau_{sm} > 0, \tau_{cb} < 0$	0	0.008	−0.008	0.008	0.014
	$\tau_{sm} < 0, \tau_{cb} > 0$	0	−0.008	0.008	−0.008	0.014
$\theta = 600$ K	$\tau_{sm} > 0, \tau_{cb} > 0$	0	0.036	−0.036	0.037	−0.065
	$\tau_{sm} < 0, \tau_{cb} < 0$	0	−0.036	0.036	−0.037	−0.065
	$\tau_{sm} > 0, \tau_{cb} < 0$	0	0.030	−0.030	0.031	0.054
	$\tau_{sm} < 0, \tau_{cb} > 0$	0	−0.030	0.030	−0.031	0.054
$\theta = 800$ K	$\tau_{sm} > 0, \tau_{cb} > 0$	0	0.046	−0.046	0.048	−0.083
	$\tau_{sm} < 0, \tau_{cb} < 0$	0	−0.046	0.046	−0.048	−0.083
	$\tau_{sm} > 0, \tau_{cb} < 0$	0	0.037	−0.037	0.038	0.067
	$\tau_{sm} < 0, \tau_{cb} > 0$	0	−0.037	0.037	−0.038	0.067

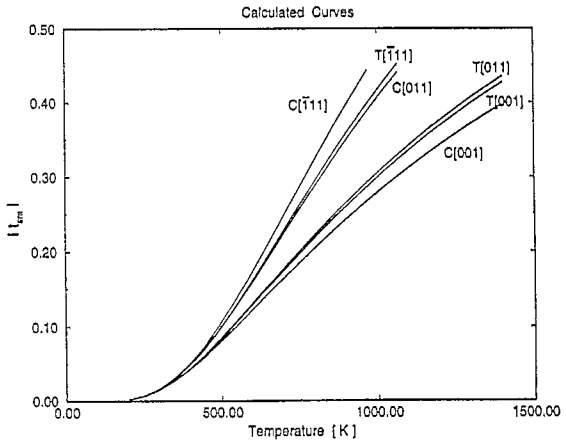

Figure 7:

Fig. 7. Normalized critical resolved shear stress $|t_{sm}|$ versus temperature θ curves obtained by the general yield criterion (Eq. (3.10)) and those estimated components of η tensor. T stands for tension and C stands for compression. The calculated curves are essentially the same as those in Fig. 13 of Paidar et al. (1984).

Fig. 7 illustrates the normalized critical resolved shear stress $|t_{sm}|$ versus temperature θ curves, obtained by the general yield criterion (Eq. (3.10)) and those estimated components of the $\boldsymbol{\eta}$ tensor, where $t_{sm} = \tau_{CRSS}/(E_1/b)$ with E_1 the APB energy on {111} planes and b the length of Burgers' vector $\boldsymbol{b}$. The calculated curves in Fig. 7 are essentially the same as those in Fig. 13 of Paidar et al. (1984). This demonstrates that the estimated $\boldsymbol{\eta}$ tensor describes, as in Paidar et al. (1984), the relative importance of each stress component contributing to flow.

4.2. Estimation of non-Schmid factors in simple metals

Asaro and Rice (1977), Chang and Asaro (1981) and Asaro (1983) have given some estimated non-Schmid factors for simple metals. Barendreght and Sharpe (1973) found in Zn single crystals η_{mm} could be as high as 0.17. Spitzig et al. (1975) had reported the *strength differential* to be as high as 0.07–0.1 in high strength martensitic steels. The strength differential, SD, is defined as the ratio $(\sigma_c - \sigma_t)/[(\sigma_c + \sigma_t)/2]$, where σ_c and σ_t are yield strengths under uniaxial compression and uniaxial tension, respectively. As pointed by Asaro and Rice (1977), the strength differential can be expressed as

$$\mathrm{SD} = \frac{4\kappa}{3}, \tag{4.1}$$

where k is the pressure sensitivity factor. If $\eta_{ss} = \eta_{mm} = \eta_{zz} = k/3$, their values are estimated to be

$$\eta_{ss} = \eta_{mm} = \eta_{zz} = \tfrac{1}{4}\mathrm{SD}. \tag{4.2}$$

Estimations and observations of non-Schmid factors for several materials are summarized in Table 2.

5. Critical conditions of localization

5.1. Bifurcation analyses for single slip

In this section, Section 5.1, we will neglect the slip system identifier subscript α, for there is only one slip system active. For example, s_1, $\boldsymbol{m}_1$ and z_1 are denoted by s, $\boldsymbol{m}$ and z respectively.

Table 2
Non-Schmid factors for some simple metals

	Zn [a]	Al–Cu [b]	Steel (martensitic) [c]	Cross-slip model [d]
η_{sz}	—	0.044	—	0.03–0.1
η_{mz}	—	—	—	0.005–0.03
η_{ss}	—	—	0.018–0.025	—
η_{mm}	~ 0.1	—	0.018–0.025	—
η_{zz}	—	—	0.018–0.025	—

[a] Data from Barendreght and Sharpe (1973).
[b] Data from Chang and Asaro (1981).
[c] Data from Spitzig et al. (1975).
[d] Theoretical results from Asaro and Rice (1979).

5.1.1. Close form solutions

Asaro and Rice (1977) have developed a rather comprehensive close form solution for the criteria that allow for bifurcation to occur under single slip. The derived criteria for bifurcation take the form of a critically low ratio of hardening rate to various measures of elastic moduli. Their perspective was that, at the points where localization occurs, hardening rates are generally decreasing functions of strain. Thus criteria were sought for the conditions where localization could occur with the largest positive hardening rate. Solutions of this kind fell into two broad categories, namely localized bands that lie nearly aligned with the slip plane (*slip band*) and those whose normals are nearly aligned with the slip direction (*kink band*). Assuming σ/L is very small (where σ stands for the order of the components of stress tensor $\boldsymbol{\sigma}$ and L stands for the order of the components of elastic moduli $\boldsymbol{L}$), Asaro and Rice (1977) have found bands that lie nearly aligned with the slip plane, but optimally oriented such that the critical hardening rate is maximized, become possible when

$$h = h_{cr} \approx \tfrac{1}{4}(\boldsymbol{\eta}:\mathscr{M}\cdot s)\cdot(s\cdot\mathscr{M}\cdot s)^{-1}\cdot(s\cdot\mathscr{M}:\boldsymbol{\eta}); \tag{5.1a}$$

these bands have the normal

$$\boldsymbol{n} \approx \boldsymbol{m} + \tfrac{1}{2}(s\cdot\mathscr{M}\cdot s)^{-1}\cdot(s\cdot\mathscr{M}:\boldsymbol{\eta}), \tag{5.1b}$$

where

$$\mathscr{M} = \boldsymbol{L} - (\boldsymbol{L}\cdot\boldsymbol{m})\cdot(\boldsymbol{m}\cdot\boldsymbol{L}\cdot\boldsymbol{m})^{-1}\cdot(\boldsymbol{m}\cdot\boldsymbol{L}). \tag{5.1c}$$

For bands whose normals are nearly aligned with the slip direction,

$$h = h_{cr} \approx \tfrac{1}{4}(\boldsymbol{\eta}:\mathscr{S}\cdot\boldsymbol{m})\cdot(\boldsymbol{m}\cdot\mathscr{S}\cdot\boldsymbol{m})^{-1}\cdot(\boldsymbol{m}\cdot\mathscr{S}:\boldsymbol{\eta}); \tag{5.2a}$$

the normal to those bands is given as

$$\boldsymbol{n} \approx s + \tfrac{1}{2}(\boldsymbol{m}\cdot\mathscr{S}\cdot\boldsymbol{m})^{-1}\cdot(\boldsymbol{m}\cdot\mathscr{S}:\boldsymbol{\eta}), \tag{5.2b}$$

where

$$\mathscr{S} = \boldsymbol{L} - (\boldsymbol{L}\cdot s)\cdot(s\cdot\boldsymbol{L}\cdot s)^{-1}\cdot(s\cdot\boldsymbol{L}). \tag{5.2c}$$

If we retain terms of order $\mathscr{O}(\sigma)$, a term $(\boldsymbol{m}\cdot\boldsymbol{\sigma}\cdot\boldsymbol{m} - s\cdot\boldsymbol{\sigma}\cdot s)$ can be added to Eq. (5.2a) for the case of a kink band, viz.,

$$h = h_{cr} \approx \tfrac{1}{4}(\boldsymbol{\eta}:\mathscr{S}\cdot\boldsymbol{m})\cdot(\boldsymbol{m}\cdot\mathscr{S}\cdot\boldsymbol{m})^{-1}\cdot(\boldsymbol{m}\cdot\mathscr{S}:\boldsymbol{\eta}) + \{\boldsymbol{m}\cdot\boldsymbol{\sigma}\cdot\boldsymbol{m} - s\cdot\boldsymbol{\sigma}\cdot s\}, \tag{5.3}$$

where the normal to the bands is still given by Eq. (5.2b). Eq. (5.3) was recently applied to model the critical conditions of kink band formation in fiber composites by Dao and Asaro (1996b).

When the elasticity is taken to be isotropic, the critical conditions of slip band Eqs. (5.1a) and (5.1b) become

$$h = h_{\mathrm{cr}} \approx G\left\{\eta_{sz}^2 + \frac{1}{4\xi}\left[(2\xi-1)\eta_{zz} + 2\xi\eta_{ss}\right]^2\right\}, \tag{5.4a}$$

with the normal to the bands given by

$$\boldsymbol{n} \approx \boldsymbol{m} + \eta_{sz} z + \frac{1}{4\xi}\left[(2\xi-1)\eta_{zz} + 2\xi\eta_{ss}\right] s; \tag{5.4b}$$

and for the case of *kink band*, (5.3) and (5.2b) become

$$h = h_{cr} \approx G\left\{\eta_{mz}^2 + \frac{1}{4\xi}\left[(2\xi-1)\eta_{zz} + 2\xi\eta_{mm}\right]^2\right\} + \{\boldsymbol{m}\cdot\boldsymbol{\sigma}\cdot\boldsymbol{m} - \boldsymbol{s}\cdot\boldsymbol{\sigma}\cdot\boldsymbol{s}\}, \tag{5.5a}$$

with the normal to the bands given by

$$\boldsymbol{n} \approx \boldsymbol{s} + \eta_{mz} z + \frac{1}{4\xi}\left[(2\xi-1)\eta_{zz} + 2\xi\eta_{mm}\right]\boldsymbol{m}. \tag{5.5b}$$

In the above,

$$\xi = (\lambda + G)/(\lambda + 2G), \tag{5.6}$$

and λ is the Lame constant and G the shear moduli. Before going into detailed analyses, it is of interest to explore the numerology of Eqs. (5.4) and (5.5); for this purpose we take Poisson's ratio $\nu = 1/3$ and hence $\xi \approx 0.7$. Noting further that for metals G is of the order 100 to $1000 g_0$, where g_0 is the initial yield stress, then if the η's in the brackets of Eq. (5.3a) are of order 0.05, then h_{cr}/G is of order 0.008 and h_{cr} itself of order $0.8 g_0$ to $8 g_0$. On the other hand, if the same η's are of order 0.01 then h_{cr}/G is of order 2×10^{-4} and h_{cr} is of order $0.02 g_0$ to $0.2 g_0$. Not only can h_{cr} be positive but for materials which have relatively large non-Schmid effects such as Ni_3Al, h_{cr} can be quite high. Similar argument applies to kink bands as well, small non-Schmid factors could make the bands appear at significant high hardening rate. On the other hand, even if we have a large non-Schmid factor, i.e. $\eta_{ss} = 0.1$, then from Eq. (5.4a) the misalignment between the slip band and the slip plane is only about 2.9°. We thus find that for single slip, while the critical hardening rate can be quite high, the misalignment of the slip band with respect to slip planes is expected to be very small. As discussed by Chang and Asaro (1981), single slip shear band modes of the type are, kinematically at least, closely related to what they termed *coarse shear band* (CSB) formation.

5.1.2. Bifurcation analyses for bands nearly aligned with the slip plane

We first define the crystal geometry as in Fig. 8. Fig. 8a shows the geometry of the slip system s, $\boldsymbol{m}$ and z and the band of localization which is defined by the band normal $\boldsymbol{n}$. Reference lab axis $\boldsymbol{X}_3$ is chosen to be aligned with z. In Fig. 8b, the normal to the band of localization $\boldsymbol{n}$ is defined by two angles, viz. ψ_1 and ψ_2; with such definitions, s can be defined as $\psi_1 = \phi$, $\psi_2 = 0°$; $\boldsymbol{m}$ can be defined as $\psi_1 = -(90° - \phi)$, and $\psi_2 = 0°$; and z as $\psi_1 = 0°$, $\psi_2 = 90°$.

5.1.2.1. General features of slip bands. For the case where the bands are nearly aligned with the slip plane, we seek solutions where $\psi_1 \approx -(90° - \phi)$ and $\psi_2 \approx 0°$. We obtain our bifurcation analyses results by solving the bifurcation Eq. (3.25) using a simple bisection numerical method, while comparisons are made with solutions estimated directly from Eqs. (5.1) or (5.4). From our calculations for $\mathscr{O}(\sigma) \ll G$, as expected, the influence of the stress state ($\boldsymbol{\sigma}$) is negligible. For the moment we assume the crystal's elasticity is isotropic with $G = 300 g_0$ and $\nu = 0.3$ where g_0 is the initial yield stress, take ϕ as 30° so that $-\psi_1 = 60°$ and $\psi_2 = 0°$ corresponds to the

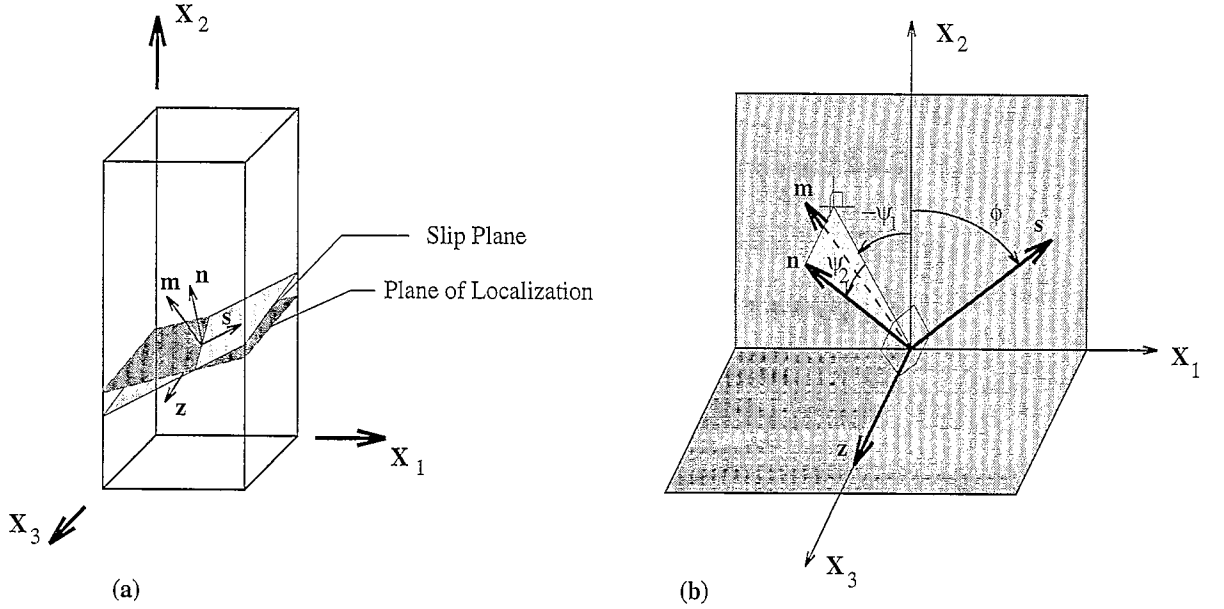

Fig. 8. (a) Geometry of the slip system s, m and z and the band of localization which is defined by the band normal n. Reference lab axis X_3 is chosen to be aligned with z. (b) The normal to the band of localization n is defined by two angles, viz. ψ_1 and ψ_2; with such definitions, s can be defined as $\psi_1 = \phi$, $\psi_2 = 0°$, m can be defined as $\psi_1 = -(90° - \phi)$, $\psi_2 = 0°$, and z can be defined as $\psi_1 = 0°$, $\psi_2 = 90°$.

slip plane normal, m. Fig. 9a shows the calculated critical hardening rate h plotted against the two angles ψ_1 and ψ_2 for the case where $\eta_{sz} = 0.06$; the highest hardening rate $h_{cr} = 1.08\,g_0$ is achieved at $-\psi_1 = 60.0°$ and $\psi_2 = 3.4°$ (which is consistent with the numbers estimated from Eq. (5.4) where $h_{cr} = 1.08\,g_0$ with $-\psi_1 = 60.0°$ and $\psi_2 = 3.4°$). Fig. 9b shows the calculated critical hardening rate h plotted against the two angles ψ_1 and ψ_2 for the case where $\eta_{ss} = 0.08$; the highest hardening rate $h_{cr} = 1.37 g_0 = \xi \eta_{ss}^2 G$ is achieved at $-\psi_1 = 57.7°$ and $\psi_2 = 0°$ (which is consistent with the numbers given by Eq. (5.4) where $h_{cr} = 1.37 g_0$ with $-\psi_1 = 57.7°$ and $\psi_2 = 0°$). It is evident that localization is possible at significantly high hardening rates and that the corresponding band of this type should closely align with the slip plane. The shape of the *surface of critical hardening rate* is nearly axisymmetric about the optimal (i.e. largest) value for h_{cr}. We notice that $\partial h/\partial\psi_1$ and $\partial h/\partial\psi_2$ are very large in terms of absolute values, which means beyond a 2 to 3 degree deviation from the optimal plane, the critical hardening rate falls quickly below zero; in this case no localization is possible unless there is significant softening. The large absolute value of $\partial h/\partial\psi_1$ and $\partial h/\partial\psi_2$ implies that the single slip shear band should be much sharper compared to the plane strain multiple slip shear band when we look ahead to Fig. 14 where $\partial h/\partial\psi_1$ is much smoother.

Additional calculations of the surface of critical hardening rate were made for different combinations of non-Schmid factors. In general it is found that: (i) when Schmid's rule holds, there is no localization possible at positive strain hardening, and, as G increases, the *cone*-shaped surface of critical hardening rate becomes sharper, i.e. the absolute values of $\partial h/\partial\psi_1$ and $\partial h/\partial\psi_2$ get larger at the same amount of deviation from the optimal position; (ii) when there are non-Schmid effects, $h_{cr} \propto G$ and if G increases the absolute values of $\partial h/\partial\psi_1$ and $\partial h/\partial\psi_2$ increase.

5.1.2.2. Influences of elastic anisotropy. Elastic constants for some simple metals and some intermetallics with cubic symmetry are listed in Table 3, where $A = 2C_{44}/(C_{11} - C_{12})$ is Zener's ratio of shear anisotropy. For a wide range of crystals, Zener's ratio of shear anisotropy, A, is usually around 1–4 and maybe as large as 8.5 for

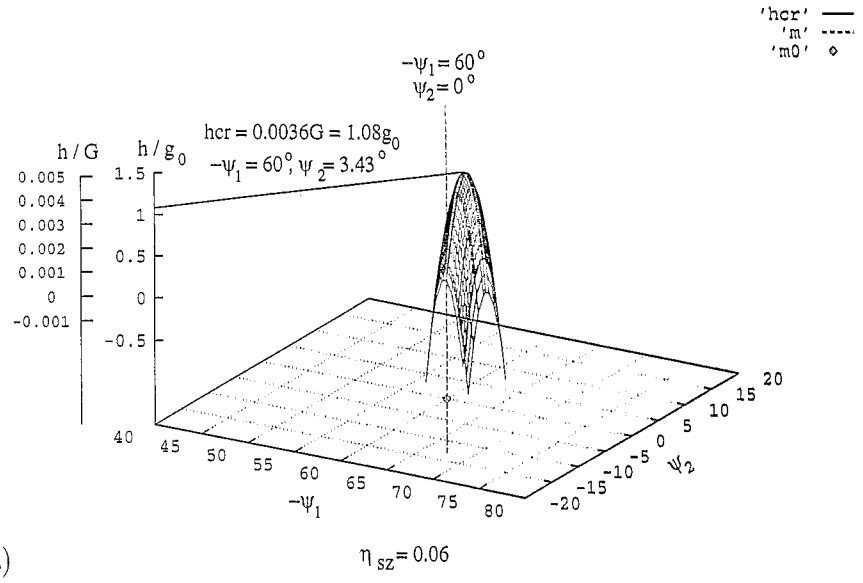

(a)

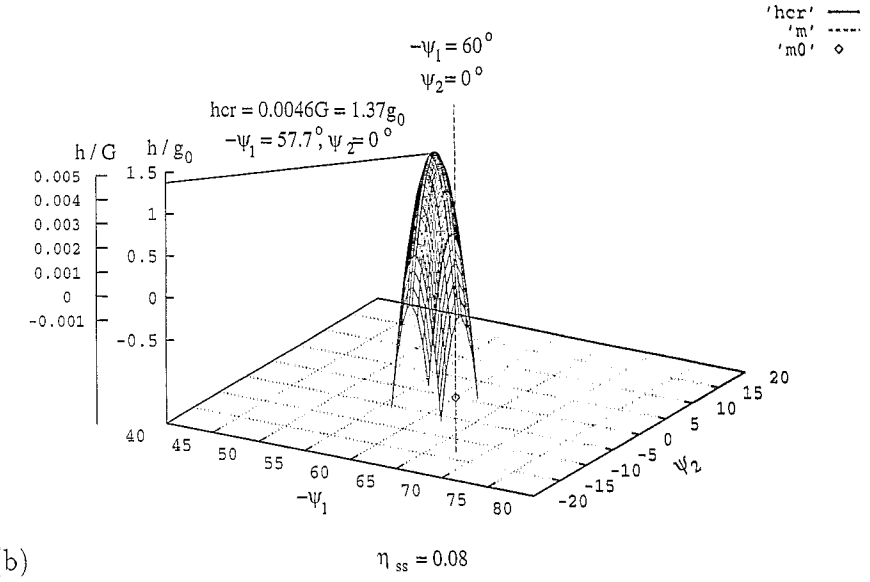

(b)

Fig. 9. (a) The calculated critical hardening rate h against the two angles ψ_1 and ψ_2 for the case that $\eta_{sz} = 0.06$, the highest hardening rate $h_{cr} = 1.08\,g_0$ is achieved at $-\psi_1 = 60.0°$ and $\psi_2 = 3.4°$; (b) the calculated critical hardening rate h against the two angles ψ_1 and ψ_2 for the case that $\eta_{ss} = 0.08$, the highest hardening rate $h_{cr} = 1.37 g_0 = \xi \eta_{ss}^2 G$ is achieved at $-\psi_1 = 57.7°$ and $\psi_2 = 0°$.

CuZn. To study the influence of the elastic anisotropy towards the critical conditions of localization in single crystals, we take the crystal axes $\boldsymbol{a}_1$, $\boldsymbol{a}_2$ and $\boldsymbol{a}_3$ to be aligned with the reference axes $\boldsymbol{X}_1$, $\boldsymbol{X}_2$ and $\boldsymbol{X}_3$ respectively. For crystals with cubic symmetry, three constants C_{11}, C_{12} and C_{44} are needed to describe the crystal elasticity. If we assume the only non-zero non-Schmid factor is η_{ss}, the normal $\boldsymbol{n}$ of the optimal localization plane lies in the plane defined by $\psi_2 = 0°$ due to symmetry; therefore the intersection line of the plane of $\psi_2 = 0°$ and the surface of critical hardening rate can obtain most of the information, including the

Table 3
Anisotropic elastic constant for some simple metals and intermetallic compounds

Material	Structure	C_{11} (GPa)	C_{12} (GPa)	C_{44} (GPa)	A
Al [a]	fcc	108.2	61.3	28.5	1.22
Au [a]	fcc	186.0	157.0	42.0	2.90
Cu [a]	fcc	168.4	121.4	75.4	3.21
Ni [a]	fcc	246.5	147.3	124.7	2.51
Fe [a]	bcc	228	132	116.5	2.43
Mo [a]	bcc	460	176	110	0.77
Ni_3Al [b]	$L1_2$	223	148	125	3.34
Cu_3Au [b]	$L1_2$	187	135	68	2.60
NiAl [b]	B2	212	143	112	3.28
CuZn [b]	B2	129	110	82	8.49

[a] Data from Kelly and Groves (1970).
[b] Data from Yoo (1987).

highest possible hardening rate and the optimal position defined by the normal $\boldsymbol{n}$. For $\eta_{ss} = 0.08$, Fig. 10 gives some results for several cases where $C_{44} = 300 g_0$ is fixed while C_{11} and C_{12} vary to give different combinations of anisotropic elasticity. We find from Fig. 10 that, (i) elastic anisotropy can have a significant influence on the critical hardening rate whereas the magnitude may vary as much as 30 to 40 percent, and (ii) while h_{cr} varies a lot with the presence of elastic anisotropy, the critical angle for the localization varies little.

We also conducted bifurcation analyses for other cases of non-Schmid effects and some of their combinations (i.e. $\eta_{sz} \neq 0$, $\eta_{zz} \neq 0$, $\eta_{sz} \neq 0$ and $\eta_{ss} \neq 0$, ...), similar results were found regarding general features of slip bands and the influences of elastic anisotropy.

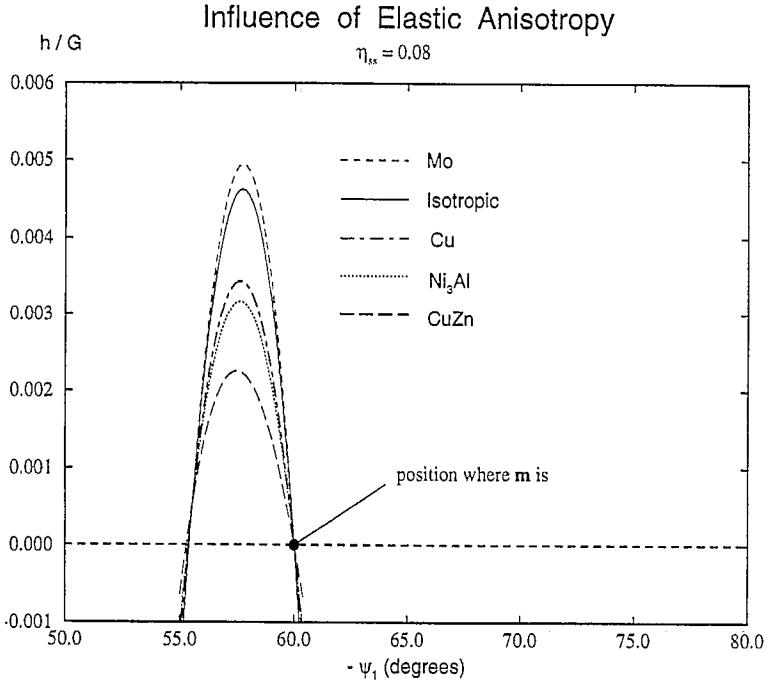

Fig. 10. Results for several cases where $C_{44} = 300 g_0$ is fixed while C_{11} and C_{12} vary to give different combinations of anisotropic elasticity. $\eta_{ss} = 0.08$ was taken for all cases.

5.1.3. Bifurcation analyses for kink bands

For the case of kink bands, the crystal geometry is again defined as in Fig. 8, where s is defined by $\psi_1 = \phi$, $\psi_2 = 0°$. Now we will seek solutions that $\psi_1 \approx \phi$ and $\psi_2 \approx 0°$. Again, we obtain our bifurcation results by solving bifurcation Eq. (3.25) using a simple bisection numerical method, while comparisons are made with solutions estimated from Eq. (5.2).

5.1.3.1. General features of kink bands. As seen in Eqs. (5.3) and (5.5a), the stress $\boldsymbol{\sigma}$ may have some influence, and the magnitude of the influence of the stress term is of order $\mathcal{O}(\sigma)$. Assume the crystal elasticity to be isotropic with $G = 300 g_0$ and $\nu = 0.3$ where g_0 is the initial yield stress, take ϕ as 30° so that $\psi_1 = 30°$ and $\psi_2 = 0°$ corresponds to the slip direction s. When under uniaxial tension with $\sigma_{22} = 2 g_0$ and $\eta_{mm} = 0.08$, the calculation of the surface of critical hardening rate plotted against the two angles ψ_1 and ψ_2 shows that the highest hardening rate $h_{cr} = 0.35 g_0$ is achieved at $\psi_1 = 27.8°$ and $\psi_2 = 0°$ (which is consistent with the numbers estimated from Eq. (5.18) where $h_{cr} = 0.37 g_0$ with $\psi_1 = 27.7°$ and $\psi_2 = 0°$); when under uniaxial compression with $\sigma_{22} = -2 g_0$ and $\eta_{mm} = 0.08$, the calculation of the surface of critical hardening rate plotted against the two angles ψ_1 and ψ_2 shows that the highest hardening rate $h_{cr} = 2.39 g_0$ is achieved at $\psi_1 = 27.6°$ and $\psi_2 = 0°$ (which is also consistent with the numbers given by Eq. (5.18) where $h_{cr} = 2.37 g_0$ with $\psi_1 = 27.7°$ and $\psi_2 = 0°$). The shape of the surfaces of critical hardening rate for the two kink band cases calculated above is found to be similar to those observed for slip bands with a nearly axisymmetric cone shape. It is evident that kink bands are possible at significantly high hardening rates, the stress state $\boldsymbol{\sigma}$ can have an important influence and bands of this type should align closely with the slip plane normal. The shape of the surface of critical hardening rate is nearly axisymmetric about the optimal position where highest possible h_{cr} is obtained. Similar to the case of the bands nearly aligned with the slip plane, $\partial h/\partial\psi_1$ and $\partial h/\partial\psi_2$ again have large absolute magnitudes.

Here both non-Schmid effects and the stress state $\boldsymbol{\sigma}$ have a significant influence on the critical conditions of localization. As an example, when s, $\boldsymbol{m}$ and $\boldsymbol{X}_2$ are within the same plane, for uniaxial loading along $\boldsymbol{X}_2$ axis, Eq. (5.5a) becomes

$$h = h_{cr} \approx G\left\{\eta_{mz}^2 + \frac{1}{4\xi}\left[(2\xi - 1)\eta_{zz} + 2\xi\eta_{mm}\right]^2\right\} - \sigma_{22}\cos 2\phi. \tag{5.7}$$

This suggests that, for this case, if $\phi < 45°$ compressive loading helps the onset of kink band and $\phi > 45°$ tensile loading helps the onset of kink band. Different non-Schmid factors and their combinations were explored, in general, it is found for kink bands that (i) stress state $\boldsymbol{\sigma}$ can influence the critical conditions of localization and (ii) similar to the case of slip bands, if G increases then h_{cr} increases and the cone-shaped surface of critical hardening rate gets sharper.

5.1.3.2. Influences of elastic anisotropy. Elastic anisotropy plays an important role here too, for example, (i) the magnitude of h_{cr} could be altered by up to 30 to 40 percent, and (ii) whereas h_{cr} varied due to elastic anisotropy, the critical angle for the localization varied little.

5.2. Bifurcation analyses for multiple slip

Although modes of deformation involving primarily single slip are often very nearly achieved in single crystals, crystalline deformation invariably occurs via activity on more than one slip systems. In polycrystals, compatibility constraints among differently oriented grains impose multiple slip system activity in all grains even under the simplest globally imposed strains. In single crystals, oriented initially for single slip, lattice rotations lead to states of multiple slip often after what typically turns out to be only modest globally imposed

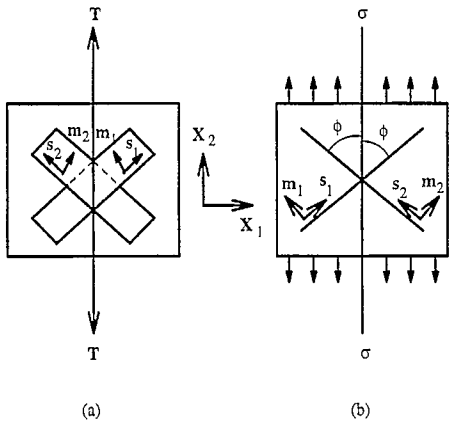

Fig. 11. Geometry for actual (a) and idealized (b) symmetric double crystalline slip. The case of a fcc crystal or a Ni_3Al single crystal oriented for symmetric primary-conjugate slip is shown in (a); note that both the tensile axis and two slip directions are in the plane of the drawing but that the two slip plane normals are tilted outward. An idealized version of (a) is shown in (b) where both slip directions and slip plane normals are in the viewing plane.

strains. Aside from global multiple slip states just mentioned, slip on other than the primary system (i.e. that on which activity is highest) can occur locally through the action of concentrated stresses developed at the tips of slip bands or at substructural sites such as dislocation boundaries. As shown by Asaro and co-workers (Asaro, 1979; Chang and Asaro, 1981; Peirce et al., 1982; Harren et al., 1988; Dao and Asaro, 1993; Dao and Asaro, 1994) multiple slip gives rise to several critical differences in phenomenology that have important implications vis-a-vis on localized plastic deformation. Two of these are the appearance of yield vertex like idealized rate-independent yield surfaces and the second is the development of geometrical softening within the deformation patterns that, in turn, induces localized plastic flow. These phenomena have been studied extensively both experimentally and theoretically in the above listed work.

5.2.1. Close form solutions

To explore localization in multiple slip, we first use a simple model to get some close form solutions incorporating non-Schmid effects and to obtain some general conclusions. Here we adopt the original model proposed by Asaro (1979) for a single crystal deforming via a primarily double mode of slip. A schematic illustration of this is shown in Fig. 11. We note there are two slip systems symmetrically oriented about the tensile axis where ϕ is the angle each slip plane makes with it; the crystal is again subject to tension along the X_2 axis.

Again we have the general hardening rule (see Eq. (3.14)):

$$\left(\boldsymbol{P}_\alpha + \boldsymbol{T}^\alpha \cdot \boldsymbol{\eta} \cdot \boldsymbol{T}^{\alpha \mathrm{T}}\right) : \overset{\triangledown}{\boldsymbol{\sigma}}{}^* = h_{\alpha\beta}\dot{\gamma}_\beta . \tag{5.8}$$

For the two-dimensional crystal model we need only keep the in-plane components of $\boldsymbol{\eta}$, viz. η_{ss} and η_{mm}. Now to account for incompressibility it is convenient to define η^+ and η^- as

$$\eta^+ = \eta_{ss} + \eta_{mm}, \qquad \eta^- = \eta_{ss} - \eta_{mm} \tag{5.9}$$

and $\boldsymbol{\eta}'$ as

$$\boldsymbol{\eta}' = \begin{pmatrix} \eta_{ss} - \frac{1}{2}\eta^+ & 0 \\ 0 & \eta_{mm} - \frac{1}{2}\eta^+ \end{pmatrix} = \begin{pmatrix} \frac{1}{2}\eta^- & 0 \\ 0 & -\frac{1}{2}\eta^- \end{pmatrix}. \tag{5.10}$$

In terms of these, Eq. (5.8) then becomes

$$\boldsymbol{Q}'_\alpha : \overset{\triangledown}{\boldsymbol{\sigma}}{}^{*} + \tfrac{1}{2}\eta^{+}\dot{p} = h_{\alpha\beta}\dot{\gamma}_\beta, \tag{5.11}$$

with

$$\boldsymbol{Q}'_\alpha = \boldsymbol{P}_\alpha + \boldsymbol{T}^\alpha \cdot \boldsymbol{\eta}' \cdot \boldsymbol{T}^{\alpha\mathrm{T}} \tag{5.12}$$

and where the pressure rate can be expressed as

$$\dot{p} = \tfrac{1}{2}\left(\overset{\triangledown}{\sigma}_{11} + \overset{\triangledown}{\sigma}_{22} \right) = \tfrac{1}{2}\left(\dot{\sigma}_{11} + \dot{\sigma}_{22}\right). \tag{5.13}$$

The development of the constitutive relations that govern this crystal follows directly and straightforwardly from the procedure found in Asaro (1979). For example, Asaro's relation (Eq. (3.15)) becomes

$$\boldsymbol{D} = \boldsymbol{L}^{-1} : \left\{ \overset{\triangledown}{\boldsymbol{\sigma}} + \boldsymbol{\sigma}\,\mathrm{tr}(\boldsymbol{D}) \right\} + \hat{\boldsymbol{P}}_\alpha N^{-1}_{\alpha\beta}\left(\boldsymbol{Q}'_\beta : \boldsymbol{L} : \boldsymbol{D}\right) + \tfrac{1}{2}\hat{\boldsymbol{P}}_\alpha \sum_\beta N^{-1}_{\alpha\beta}\eta^{+}\dot{p}, \tag{5.14}$$

where

$$N_{\alpha\beta} = h_{\alpha\beta} + \boldsymbol{Q}'_\alpha : \boldsymbol{L} : \boldsymbol{P}_\beta. \tag{5.15}$$

To complete the constitutive analysis we next assume that the crystal's elasticity is isotropic and incompressible; this has the effect of simplifying the relations and preserving the phenomena. Then $\mathrm{tr}(\boldsymbol{D}) = 0$ and the first term in Eq. (5.14) becomes

$$\frac{1}{2G}\overset{\triangledown}{\sigma},$$

where G is the elastic shear modulus. We next, as in Asaro (1979), take $h_{\alpha\beta}$ to have the elements $h_{11} = h_{22} = h$ and $h_{12} = h_{21} = h_1$, and write tensile stress $\sigma = \sigma_{22}$. Together those yield for $N^{-1}_{\alpha\beta}$

$$N^{-1}_{\alpha\beta} = \frac{1}{\det N}\begin{pmatrix} h + G & -h_1 + G\cos 4\phi - G\eta^{-}\sin 4\phi \\ -h_1 + G\cos 4\phi - G\eta^{-}\sin 4\phi & h + G \end{pmatrix}, \tag{5.16}$$

and finally

$$D_{11} = \frac{1}{2G}\overset{\triangledown}{\sigma}_{11} - \frac{G\sin 2\phi(\sin 2\phi + \eta^{-}\cos 2\phi)}{\left(h + h_1 + 2G\sin^2 2\phi + G\eta^{-}\sin 4\phi\right)}\left(D_{22} - D_{11}\right) - \frac{\delta\dot{p}}{2G}, \tag{5.17a}$$

$$D_{22} = \frac{1}{2G}\overset{\triangledown}{\sigma}_{22} + \frac{G\sin 2\phi(\sin 2\phi + \eta^{-}\cos 2\phi)}{\left(h + h_1 + 2G\sin^2 2\phi + G\eta^{-}\sin 4\phi\right)}\left(D_{22} - D_{11}\right) + \frac{\delta\dot{p}}{2G}, \tag{5.17b}$$

$$D_{12} = \frac{1}{2G}\overset{\triangledown}{\sigma}_{12} + \frac{G(2\cos 2\phi - \sigma/G)(\cos 2\phi - \eta^{-}\sin 2\phi)}{\left(h - h_1 + 2G\cos^2 2\phi - G\eta^{-}\sin 4\phi\right)}D_{12}, \tag{5.17c}$$

along with the incompressible constraint, viz.

$$D_{11} + D_{22} = 0. \tag{5.17d}$$

δ is defined as

$$\delta = \frac{2G\eta^{+}\sin 2\phi}{\left(h + h_1 + 2G\sin^2 2\phi + G\eta^{-}\sin 4\phi\right)}. \tag{5.18}$$

Alternatively, the above relations may be rephrased in a form used to study the influence of pressure sensitivity in bifurcation within the plane strain tension by Needleman (1979), viz.

$$\overset{\nabla}{\sigma}_{11} = 2\mu^* D_{11} + (1+\delta)\dot{p}, \tag{5.19a}$$

$$\overset{\nabla}{\sigma}_{22} = 2\mu^* D_{22} + (1-\delta)\dot{p}, \tag{5.19b}$$

$$\overset{\nabla}{\sigma}_{12} = 2\mu D_{12}, \tag{5.19c}$$

and again

$$D_{11} + D_{22} = 0. \tag{5.19d}$$

To make specific contact with the plane strain incompressible forms used by Hill and Hutchinson (1975), and for the single crystal by Asaro (1979), the first two of Eqs. (5.19) are combined to yield

$$\overset{\nabla}{\sigma}_{22} - \overset{\nabla}{\sigma}_{11} = 2\mu^*(D_{22} - D_{11}) - 2\delta\dot{p}. \tag{5.20}$$

In the above

$$2\mu^* = \frac{2G(h+h_1)}{\left(h+h_1+2G\sin^2 2\phi + G\eta^- \sin 4\phi\right)}, \tag{5.21a}$$

$$2\mu = \frac{2G(h-h_1+\sigma\cos 2\phi - \sigma\eta^- \sin 2\phi)}{\left(h-h_1+2G\cos^2 2\phi - G\eta^- \sin 4\phi\right)}. \tag{5.21b}$$

Note that when $G \gg \sigma$, $G \gg h$ and $G \gg h_1$, we have

$$2\mu^* = \frac{h+h_1}{\sin^2 2\phi + \eta^- \sin 2\phi \cos 2\phi}, \tag{5.22a}$$

$$2\mu = \frac{h-h_1+\sigma\cos 2\phi - \sigma\eta^- \sin 2\phi}{\cos^2 2\phi - \eta^- \sin 2\phi \cos 2\phi}, \tag{5.22b}$$

and

$$\delta = \frac{\eta^+}{\sin 2\phi + \eta^- \cos 2\phi}. \tag{5.22c}$$

When the bifurcation conditions listed in Eqs. (3.18) and (3.19) are applied to the above constitutive equations, the consistency criterion for localization takes the form

$$(1+\delta)\left(\mu - \tfrac{1}{2}\sigma\right)n_1^4 + \{2(2\mu^* - \mu) - \delta\sigma\}n_1^2 n_2^2 + (1-\delta)\left(\mu + \tfrac{1}{2}\sigma\right)n_2^4 = 0, \tag{5.23}$$

where $\boldsymbol{n}$ is again the normal to the shear band and σ is the tensile stress. Writing $n_1^2 = \cos^2(\theta)$ and $n_2^2 = \sin^2(\theta)$ in Eq. (5.23), using Eqs. (5.22a) and (5.22b), we have the close form solution

$$\frac{h}{\sigma} = \frac{\cos 2\theta - \cos^2 2\theta/\cos 2\phi + \delta(1 - \cos 2\theta/\cos 2\phi)}{(1-q)\cos^2 2\theta/B + (1+q)\sin^2 2\theta/A + (1-q)\delta\cos^2 2\theta/B}, \tag{5.24a}$$

where

$$A = \sin^2 2\phi + \eta^- \sin 2\phi \cos 2\phi, \tag{5.24b}$$

$$B = \cos^2 2\phi - \eta^- \sin 2\phi \cos 2\phi, \tag{5.24c}$$

$$q = h_1/h, \tag{5.24d}$$

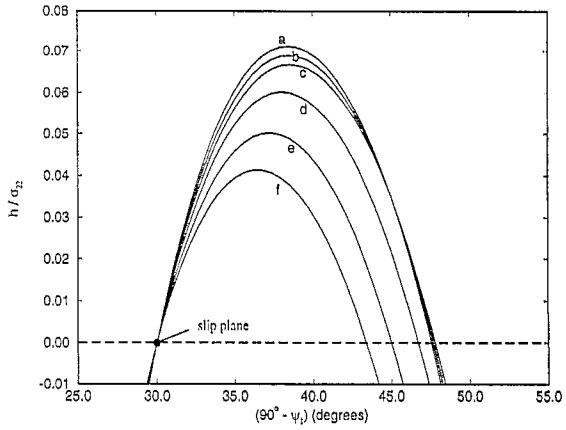

Fig. 12. The critical ratio $(h/\sigma)_{cr}$ for a band of localized shear inclined by the angle θ is shown for the case of $\phi = 30°$. Several sets of non-Schmid factors are taken as (a) $\eta_{ss} = 0.08$ $\eta_{mm} = 0$, (b) $\eta_{ss} = 0.04$ $\eta_{mm} = 0.04$, (c) $\eta_{ss} = 0$ $\eta_{mm} = 0.08$, (d) $\eta_{ss} = 0$ $\eta_{mm} = 0.05$, (e) $\eta_{ss} = 0$ $\eta_{mm} = 0$ and (f) $\eta_{ss} = 0$ $\eta_{mm} = -0.05$, respectively.

and δ is given by Eq. (5.22c). When Schmid's rule holds, i.e. $\eta^+ = 0$ and $\eta^- = 0$ so that $\delta = 0$, Eq. (5.24a) is reduced to

$$\frac{h}{\sigma} = \frac{\cos 2\theta - \cos^2 2\theta/\cos 2\phi}{(1-q)\cos^2 2\theta/\cos^2 2\phi + (1+q)\sin^2 2\theta/\sin^2 2\phi}, \tag{5.25}$$

which is the same as given by Asaro (1979). Nemat-Nasser et al. (1981) had given a quite general extension of Asaro's model, in that they included both the pressure sensitivity and the plastic volume change. A slightly different form of Eq. (5.23) was developed (Nemat-Nasser et al., 1981).

For a crystal of this type undergoing multiple slip, the critical conditions for bifurcation take the form of critical ratios of hardening rate to tensile stress, σ; examples are shown for various combinations of the parameters η_{ss} and η_{mm} in Fig. 12. Note that the curve marked 'e', pertaining to the case where $\eta_{ss} = \eta_{mm} = 0$, was originally shown by Asaro (1979). The effects of deviations from Schmid's rule are significant in that when $\eta_{ss} + \eta_{mm} \approx 0.08$, for example, the critical hardening rates to stress ratios can be nearly 30–40 percent larger. In this particular orientation the optimal orientation of the bands is affected only slightly, although a range of band orientations under conditions where h is positive is distinctly possible. We noted that, (i) h_{cr} for multiple slip is of order $0.1\,g_0 \sim 0.5\,g_0$ (say, for the sake of discussion, take a reasonable number as $\sigma = \sigma_{22} = 2 \sim 3\,g_0$), while h_{cr} for single slip with some non-Schmid effects is of order $g_0 \sim 5\,g_0$; (ii) the absolute value of $\partial h/\partial\psi_1$ in multiple slip case is much smoother than the case of single slip, suggesting that the multiple slip band would be less sharper than the single slip band.

5.2.2. Three-dimensional bifurcation analysis for multiple slip

The geometry of double slip in three dimensions is divided into three types. Fig. 13 shows three different slip geometries. The first is characterized by having the line of intersection between the two slip planes perpendicular to both slip directions s_1 and s_2 (Fig. 13a); the second is characterized by having the two slip directions s_1 and s_2 symmetric about, but not perpendicular to, the line of intersection between the two slip planes (Fig. 13b); the third is characterized by the two slip directions s_1 and s_2 not symmetric about the line of intersection between the two slip planes (Fig. 13c). Type I may represent the case of bcc crystals with two $\langle 111\rangle\{\bar{2}11\}$ slip systems active; type II may represent the case of fcc crystals with two $\langle 01\bar{1}\rangle\{111\}$ slip systems active; type III may represent the case of HCP crystals with two different types of slip systems active, i.e. basal and prismatic slip. To study the localization conditions in three dimensions, we will focus our effort on the first

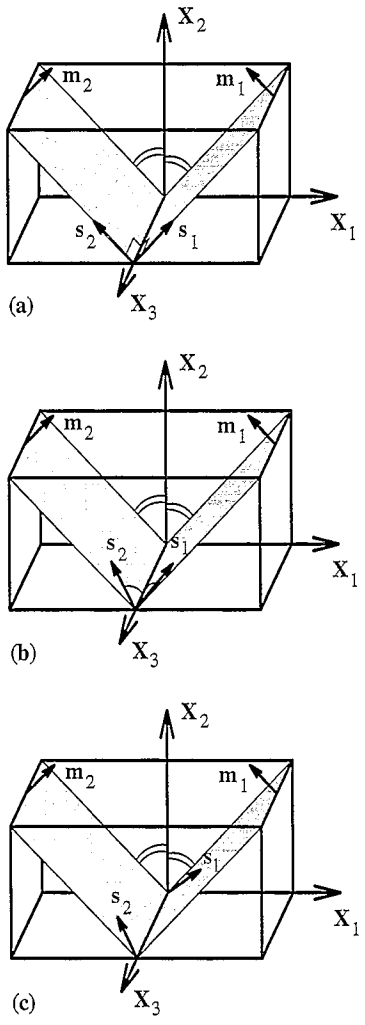

Fig. 13. The geometry of double slip in three dimension can be divided into three types: (a) the intersection line of the two slip planes is perpendicular to both of the slip directions s_1 and s_2, (b) the two slip directions s_1 and s_2 are symmetric about but not perpendicular to the intersection line of the two slip planes, and (c) the two slip directions s_1 and s_2 are not symmetric about the intersection line of the two slip planes.

two types of slip geometry which are most common for bcc, fcc and intermetallic compounds, although the general method presented in Section 5.1 can be applied for any slip geometry including type III and those cases where more than two slip systems are active.

5.2.2.1. Type I geometry multiple slip shear bands

General features of type I geometry shear bands. Now for the case of the type I geometry, we define our reference lab axes to be X_1, X_2 and X_3 where X_3 is parallel to the line of intersection between the two slip planes and s_1 and s_2 are symmetric with respect to X_2 (see Fig. 13a). The normal n to the plane of localization is again defined by two angles ψ_1 and ψ_2 as seen in Fig. 8b. When under uniaxial loading with X_2 being the loading direction, this is actually a perfect plane strain geometry which is the same as that defined in Section 5.2.1. Noting that for this double slip geometry, g in Eq. (3.18) has to be within the plane determined by s_1 and s_2 or only small perturbations allowed. We thus expect solutions such that ψ_2 is small. Fig. 14 shows a

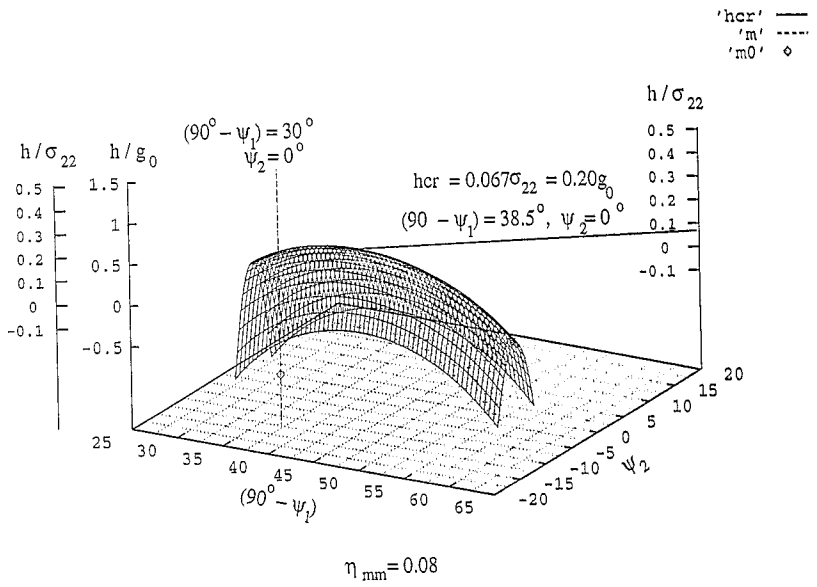

Fig. 14. A three-dimensional bifurcation analysis where the non-Schmid effects is taken as $\eta_{mm} = 0.08$ for both slip systems, and the elasticity is taken as isotropic with $G = 300 g_0$ and $\nu = 0.3$. The highest possible hardening rate $h_{cr} = 0.20 g_0 = 0.067\sigma_{22}$ is achieved at $\psi_1 = 41.5°$ ($90° - \psi_1 = 38.5°$) and $\psi_2 = 0°$.

three-dimensional bifurcation analysis where the non-Schmid effects is taken as $\eta_{mm} = 0.08$ for both slip systems; the elasticity is taken as isotropic with $G = 300 g_0$ and $\nu = 0.3$, the stress state is uniaxial with $\sigma_{22} = 3 g_0$. The highest possible hardening rate $h_{cr} = 0.20 g_0 = 0.067\sigma_{22}$ is achieved at $\psi_1 = 41.5°$ ($90° - \psi_1 = 38.5°$) and $\psi_2 = 0°$, which is consistent with the numbers given by Eq. (5.24) where $h_{cr} = 0.067\sigma_{22}$ with $\psi_1 = 38.5°$. A symmetric solution can be found for the conjugate slip system. This critical hardening rate is about 30 percent higher than that for the case where Schmid's rule holds. It is evident that for the case of double slip the optimal plane deviates much more from the slip plane than that for the case of single slip. Also it is very interesting to observe that while $\partial h/\partial\psi_2$ remains quite steep $\partial h/\partial\psi_1$ is very smooth as compared with the single slip mode (i.e., compare Fig. 14 with Fig. 9a and b). This suggests that this double slip deformation mode may have bands that are broader than the single slip bands.

When σ_{22} varies at the onset of localization for different materials, we find that (h_{cr}/σ_{22}) remains constant although $\partial h/\partial\psi_1$ slightly changes along the surface of critical hardening rate. If we vary the elastic moduli $\boldsymbol{L}$, as long as $\mathscr{E}(\boldsymbol{L}) \gg \sigma_{22}$, (h_{cr}/σ_{22}) remains constant. Thus we conclude that, for the type I double slip geometry, the critical condition takes the form $h_{cr} = F(\sigma_{22}$, non-Schmid effects).

To summarize the general features for type I geometry double slip shear bands, (i) the critical shear band angle is typically several degrees (≈ 7–$10°$) misoriented from the active slip planes; (ii) non-Schmid effects have a significant influence on the critical hardening rate h_{cr}, while critical shear band angle is not strongly affected by non-Schmid effects; (iii) the surface of critical hardening rate is much less sharp as compared to the surface for single slip shear bands.

Influences of elastic anisotropy. When we take the crystal axes $\boldsymbol{a}_1$, $\boldsymbol{a}_2$ and $\boldsymbol{a}_3$ along with $\boldsymbol{X}_1$, $\boldsymbol{X}_2$ and $\boldsymbol{X}_3$, for crystals with cubic symmetry, unlike the single slip case the elastic anisotropy does not affect the critical conditions for localization although $\partial h/\partial\psi_2$ slightly changes along the surface of critical hardening rate.

Influences of non-symmetric loading. We next explore the influence of non-symmetric loading conditions, i.e. those cases where the primary and conjugate slip systems are not symmetrically loaded. Let the uniaxial loading axis deviate along ψ_2 away from the perfect plane strain case where the loading direction was defined

by $\psi_1 = 0°$ and $\psi_2 = 0°$. If we let the deviation be $\psi_2 = \Delta$ (Δ was taken between 0–30°), the uniaxial stress be again denoted by σ, it is found that the critical conditions depend only on the tensile stress along X_2 axis $\sigma_{22} = \sigma \cos^2\Delta$.

When we let the uniaxial loading axis deviate along ψ_1, the geometry is no longer symmetric. There are many cases where both the conjugate slip system and the primary system are active at the same time while the slip geometry is not symmetric. This might be the case when the latent hardening ratio is smaller than unity, or when there is overshoot for the case where latent hardening ratio is larger than unity. For cases where Schmid's rule holds and where the non-zero non-Schmid factors are η_{ss}, η_{mm} or η_{zz}, the critical hardening rate will be on the plane defined by $\psi_2 = 0$ due to the symmetry. We thus let the loading axis tilt 2° from the symmetric position, i.e. the loading axis defined by $\psi_1 = \Delta = 2°$ (and $\psi_2 = 0°$). Fig. 15a shows the critical ratio h/σ (where σ is the tensile stress along the tilted loading axis) plotted against $90° - \psi_1$ for the primary and conjugate slip system respectively, the solid line is the case where loading is symmetric; the elasticity is taken as isotropic with $\nu = 0.3$ and Schmid's rule holds for plastic yielding. Fig. 15b shows the critical ratio h/σ plotted against $90° - \psi_1$ for the primary and conjugate slip system respectively, the solid line is the case where loading is symmetric; the elasticity is taken as isotropic with $\nu = 0.3$ and non-Schmid effects are taken with $\eta_{ss} = 0.08$. Fig. 15c shows the critical ratio h/σ plotted against $90° - \psi_1$ for the primary and conjugate slip system respectively, the solid line is the case where loading is symmetric; the elasticity is taken as isotropic and incompressible, and Schmid's rule holds for plastic yielding. We note that small deviations from the symmetric axis can result in significant increases in the critical hardening rate for the conjugate slip system. This means that for the cases when the loading axis is close to the symmetric axis the major macroscopic shear band may tend to form on the conjugate slip system. From Fig. 15a and b, the strong influence of non-Schmid effects towards the critical hardening rate is apparent. From comparing Fig. 15a and c, it is evident that elastic constants have an important influence on the critical conditions, especially under non-symmetric loading. It is therefore concluded that, under symmetric loading incompressible elasticity idealization works perfect whereas under non-symmetric loading incompressible elasticity idealization is not accurate.

Similar results were obtained for $\eta_{ss} \neq 0$ and/or $\eta_{zz} \neq 0$ that these non-Schmid effects may also significantly increase the critical hardening rate h_{cr} for as much as 30 to 40 percent while the bands deviates from the slip plane several degrees (7–10°), the results take the form of the critical ratio of h/σ_{22} and elastic anisotropy does not have first order influence on the results.

5.2.2.2. Type II geometry multiple slip shear bands. For the type II geometry shown in Fig. 13b, we will focus on the fcc type of geometry, i.e. two $\langle 01\bar{1}\rangle\{\bar{2}11\}$ slip systems active. Let $[\bar{1}01](111)$ and $[011](\bar{1}\bar{1}1)$ to be the primary and conjugate slip system, respectively, define $X_1 = [110]$, $X_2 = [001]$ and $X_3 = [1\bar{1}0]$ for convenience (see Fig. 16). The normal n to the plane of localization is again defined by two angles ψ_1 and ψ_2 as seen in Fig. 8b.

General features of type II geometry shear bands. When under uniaxial loading with $[\bar{1}12]$ the loading direction, the deformation mode is double symmetric slip. Fig. 17 shows the results of a three-dimensional bifurcation analysis where the non-Schmid effects are taken as $\eta_{sz} = -0.06$ for both slip systems; the elasticity is taken as isotropic with $G = 300 g_0$ and $\nu = 0.3$, the latent hardening ratio is taken as $q = 1$ and the stress state is uniaxial with tensile stress to be $2g_0$ along $[\bar{1}12]$. The highest possible hardening rate, $h_{cr} = 1.17 g_0$, is achieved at $90° - \psi_1 = 36.8°$ ($\psi_1 = 53.2°$) and $\psi_2 = 3.1°$ which is very close to m_1 ($\psi_1 = 54.7°$ and $\psi_2 = 0°$). The result shown is for primary slip system, and a symmetric solution can be found for the conjugate slip system. Localization may occur under positive hardening is clearly shown. The order of h_{cr} is similar to what is obtained from the single slip analyses, i.e. of order $g_0 \sim 5g_0$. The absolute values of $\partial h/\partial\psi_1$ and $\partial h/\partial\psi_2$ are both quite large which is similar to the single slip case. It is very unlikely that localized deformation will persist at the same location if the material strain hardening is of order $g_0 \sim 5g_0$. Therefore coarse slip bands may form if the critical conditions are met for this case. Symmetric solutions for *both* primary and conjugate slip systems suggest that for many cases the coarse shear bands tend to appear on both primary and conjugate slip systems at

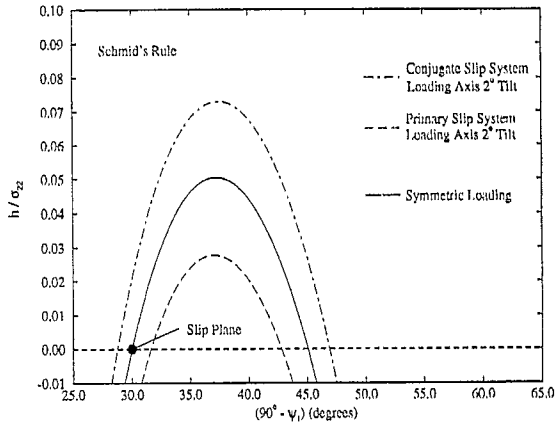

Fig. 15. Results obtained under non-symmetric loading, where (a) Schmid's rule with isotropic elasticity ($\nu = 0.3$), (b) $\eta_{33} = 0.08$ with isotropic elasticity ($\nu = 0.3$), and (c) Schmid's rule with isotropic incompressible elasticity, were taken respectively.

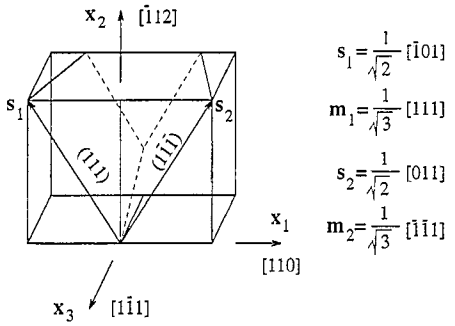

Fig. 16. Geometry in fcc type of crystals under $[\bar{1}01](111)$ and $[011](\bar{1}\bar{1}1)$ primary-conjugate double slip.

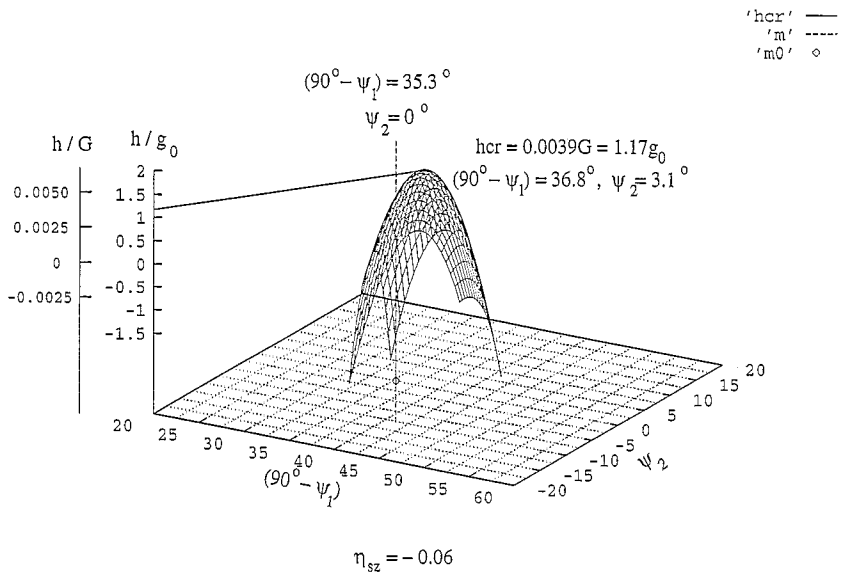

Fig. 17. A three-dimensional bifurcation analysis where the non-Schmid effects are taken as $\eta_{sz} = -0.06$ for both slip systems; the elasticity is taken as isotropic with $G = 300g_0$ and $\nu = 0.3$, latent hardening ratio is taken as $q = 1$ and the stress state is uniaxial tension. The highest possible hardening rate $h_{cr} = 1.17g_0$ achieved at $90° - \psi_1 = 36.8°$ ($\psi_1 = 53.2°$) and $\psi_2 = 3.1°$, which is very close to $\boldsymbol{m}_1$ ($\psi_1 = 54.7°$ and $\psi_2 = 0°$).

the same time. When there are no non-Schmid effects, i.e. Schmid's rule holds, our bifurcation analysis shows that localization is not possible unless there is material softening or perfect plasticity.

The case for this geometry with $\eta_{sz} = -0.06$ is very similar to the case of single slip in a sense that elastic constants including elastic anisotropy play an important role here and critical hardening rate is almost proportional to the elastic constants ($h_{cr}/G \sim$ const. for a specific material), although the stress terms (σ) do have some small influences ($< 10\%$). Similar results were obtained for other η's when they were not zero, η_{zz} was found to have similar order of influence as η_{sz} while the influences of η_{ss}, η_{mm} and η_{mz} were found to be an order of magnitude lower than those of η_{sz} and η_{zz}.

In short, for type II multiple slip shear bands, (i) when Schmid's rule holds, there is no localization possible at positive strain hardening, and, if G increases, the cone-shaped surface of critical hardening rate becomes sharper, i.e. $\partial h/\partial\psi_1$ and $\partial h/\partial\psi_2$ become larger; (ii) when there are non-Schmid effects, $h_{cr} \propto G$ and if G increases, $\partial h/\partial\psi_1$ and $\partial h/\partial\psi_2$ become larger which means sharper cone-shaped surface of critical hardening rate; (iii) elastic anisotropy is an important factor, where critical hardening rate could be changed as much as

30–40% while no significant changes were observed with critical orientations of the shear bands; (iv) η_{sz} and η_{zz} were found to have similar influences towards the critical hardening rate, while influences of η_{ss}, η_{mm} and η_{mz} were found to be an order of magnitude lower. We must emphasize here that, for crystals deforming in a multiple slip mode, non-uniform lattice rotations and *geometric softening* may play a very important role, therefore multiple slip shear bands of this type may initiate on planes very close to the active slip planes and rotate away once the bands persist at the same location.

Influences of non-symmetric loading. We next study the influence of non-symmetric loading conditions, i.e. those cases where the primary and conjugate slip systems are not symmetrically loaded. First, we let the uniaxial loading axis deviate along ψ_2 away from the perfect plane strain case where the loading direction is defined by $\psi_1 = 0°$ and $\psi_2 = 35.3°$ ([$\bar{1}$12]). Let the deviation be $\psi_2 = 35.3° + \Delta$, it is found that h_{cr} varies with different Δ's, but usually less than 10 percent.

When we let the uniaxial loading axis deviate along ψ_1, the geometry is no longer symmetric. Again, if the conjugate slip system becomes active before the primary system rotates to the symmetry boundary ($q < 1$) or when there is overshoot ($q > 1$), this type of double slip geometry should be the case. When loading axis varies with ψ_1 (while $\psi_2 = 35.3°$ is fixed), the critical hardening rate is achieved on the plane defined by $\psi_2 = 3.1°$. We thus plot our results on the $\psi_2 = 3.1°$ plane for the three-dimensional bifurcation analysis. Let the loading axis be tilted 4° from the symmetric position, i.e. the loading axis is defined by $\psi_1 = 4°$ (and $\psi_2 = 35.3°$). Fig. 18a shows the critical ratio h/G plotted against $90° - \psi_1$ for the primary and conjugate slip system respectively; the solid line is the case where loading is symmetric. The elasticity is taken as isotropic with $G = 300 g_0$ and $\nu = 0.3$; Schmid's rule is used for plastic yielding. It is found that when Schmid's rule holds localization is very unlikely to occur at relatively high strain hardening rates where CSB's usually appear. Fig. 18b shows critical ratio h/G plotted against $90° - \psi_1$ for the primary and conjugate slip system, respectively. The solid line is the case where loading is symmetric. The elasticity is taken as isotropic with $G = 300 g_0$ and $\nu = 0.3$; non-Schmid effects are taken such that $\eta_{sz} = -0.06$. We note deviations from the symmetric position actually promote shear bands that are close to the conjugate slip system (where resolved shear stress is smaller); whereas the difference between the critical hardening rates for the primary and conjugate slip systems is fairly small, suggesting two sets of shear bands may exist simultaneously. This is in agreement with the experimental results. Chang (1979) and Price and Kelly (1964) both observed that for many cases CSB's appeared first on the conjugate slip system, and two sets of CSB's belonging to different slip systems may be observed simultaneously.

5.3. Summary of bifurcation analyses and comparison with experimental observations

To summarize our bifurcation analyses, Table 4 shows some selected results we have calculated under uniaxial tension, where for all the isotropic elasticity cases, the elasticity was taken as $G = 300 g_0$ and $\nu = 0.3$, and where for the single slip modes and double slip modes the tensile stress σ_{22} was taken as $2 g_0$ and $3 g_0$, respectively.

As speculated by Price and Kelly (1964), among others, CSB's can only form at relatively high hardening rates where the localized deformation modes are not persistent. This argument is confirmed in Part II of this series (Dao and Asaro, 1996a). Therefore relatively high optimal critical hardening rate may be a good indicator to identify cases where CSB's can form first before the formation of MSB's. As our calculations in Part II (Dao and Asaro, 1996a) suggest, h_{cr} of order g_0 may lead to CSB localization pattern. With that in mind, we conclude that for CSB's:

(1) With moderate non-Schmid effects (non-Schmid factors as low as 0.04, easily unnoticed during experimental verifications of the Schmid rule), CSB's are possible in both single slip mode and double slip mode (type I and type II geometry); when Schmid's rule holds, CSB's are not possible.

(2) In single slip mode, i.e. $\eta_{ss} \neq 0$ or $\eta_{sz} \neq 0$, CSB's can form on planes that are almost parallel to the primary slip plane; misorientation between shear bands and primary slip plane is usually no larger than 3°.

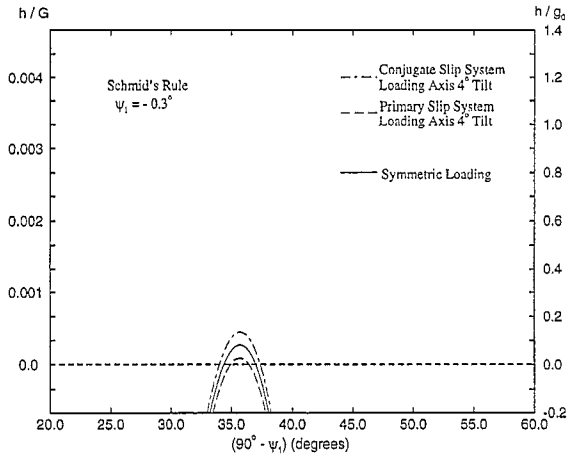

(a)

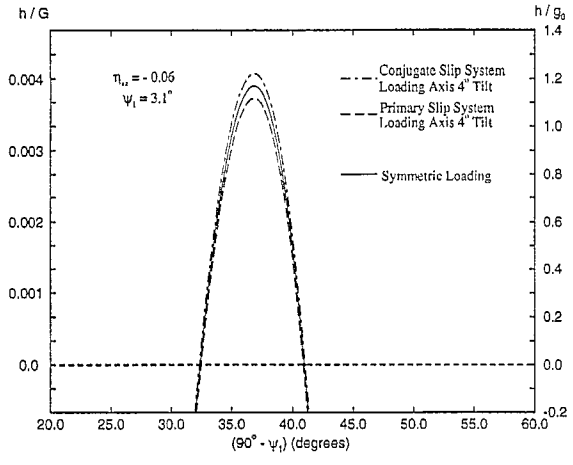

(b)

Fig. 18. (a) The critical ratio h/G against $90° - \psi_1$ for the primary and conjugate slip system, respectively. The solid line is the case where loading is symmetric; the elasticity is taken as isotropic with $\nu = 0.3$ and Schmid's rule holds for plastic yielding. (b) The critical ratio h/G against $90° - \psi_1$ for the primary and conjugate slip system, respectively. The solid line is the case where loading is symmetric; the elasticity is taken as isotropic with $\nu = 0.3$ and non-Schmid effects are taken with $\eta_{sz} = -0.06$.

(3) In double slip mode, i.e. $\eta_{sz} \neq 0$ in type I geometry and $\eta_{zz} \neq 0$ or $\eta_{sz} \neq 0$ in type II geometry, CSB's can form on planes that are almost parallel to either the primary slip plane or the conjugate slip plane; CSB's that are almost parallel to the conjugate slip plane are favored, while the critical hardening rates for the primary and conjugate slip system is fairly small, suggesting two sets of shear bands belonging to different slip systems may exist simultaneously; misorientation between shear bands and the active slip planes is usually small (3°–4°), but may go as high as 5°–7° if there is significant non-Schmid factor η_{zz} in type II geometry.

The above listed theoretical predictions regarding CSB formation, agree very well with existing experimental observations mentioned and summarized in Section 2.

As of MSB's, when the deformation gets larger, we expect there will be more than one slip system operating within the shear bands. There are two possible origins of MSB: (a) starting first with a persisting single slip shear band which is almost parallel to the primary slip plane; as deformation gets larger conjugate slip system is

Table 4
Selected results of shear bands for different deformation modes and slip geometry

	Deformation mode	h_{cr}	Misorientation	Influence of elastic anisotropy	Influence of nonsymmetric loading
Schmid's rule	single slip	0	0°	—	—
	double slip (type I)	$0.15g_0$	7.4°	no	favor conjugate
	double slip (type II)	$0.080g_0$	0.6°	yes	favor conjugate
$\eta_{ss} = 0.04$–0.08	single slip	0.34–$1.37g_0$	1.2°–2.3°	yes	—
	double slip (type I)	0.18–$0.21g_0$	7.9°–8.5°	no	favor conjugate
	double slip (type II)	0.15–$0.30g_0$	1.2°–2.3°	yes	favor conjugate
$\eta_{mm} = 0.04$–0.08	single slip	0	0°	—	—
	double slip (type I)	0.17–$0.20g_0$	7.9°–8.6°	no	favor conjugate
	double slip (type II)	0.086–$0.091g_0$	0.6°–0.6°	yes	favor conjugate
$\eta_{zz} = 0.04$–0.08	single slip	0.03–$0.13g_0$	0.3°–0.7°	yes	—
	double slip (type I)	0.17–$0.18g_0$	7.5°–8.1°	no	favor conjugate
	double slip (type II)	0.46–$1.34g_0$	3.7°–7.3°	yes	favor conjugate
$\eta_{sz} = -0.04$–-0.08	single slip	0.48–$1.92g_0$	2.3°–4.6°	yes	—
	double slip (type I)	0.52–$1.91g_0$	3.2°–4.5°	no	favor conjugate
	double slip (type II)	0.56–$2.02g_0$	2.3°–4.6°	yes	favor conjugate
$\eta_{mz} = 0.03$–0.05	single slip	0	0°	—	—
	double slip (type I)	0.16–$0.17g_0$	7.6°–8.6°	no	favor conjugate
	double slip (type II)	0.077–$0.075g_0$	0.6°–0.6°	yes	favor conjugate

activated, and the lattice within the shear band will gradually rotate away from the surrounding lattice, which can result in geometrical softening and the band itself will rotate further away from the primary slip plane; (b) starting with a type I or type II geometry double slip shear band, where MSB's can form on planes close to either the primary slip plane or the conjugate slip plane with bands close to the conjugate slip plane a little favored; as the band fully develops, the lattice within the shear band will rotate away from the surrounding lattice, which may result in geometrical softening and the band itself will rotate further away from the primary slip plane or the conjugate slip plane. After reviewing our results in Table 4, we thus conclude that, for MSB's:

(1) the well developed MSB's from either origin (a) or (b) will be typically several degrees misoriented from the active slip planes — primary or conjugate;

(2) MSB's may start on planes close to either primary or conjugate slip plane;

(3) non-Schmid effects can have significant influence toward the critical localization conditions;

(4) when Schmid's rule holds, MSB's are possible with low but positive hardening under multiple slip modes, while there is no shear banding possible with positive hardening under single slip mode.

The above mentioned theoretical predictions regarding MSB's agree well with previous experimental documentations that are summarized in Section 2.

6. Discussion

Localized deformation may lead very quickly to ductile failure; therefore to determine quantitatively the critical localization conditions (i.e., h_{cr} and shear band orientation) is very important. From the results obtained in this study, it is again evident that localization is possible while material is strain hardening. Consistent with existing experimental observations regarding CSB and MSB formation, our results obtained and summarized in Section 5 provide some explanations towards several outstanding questions, e.g.: (i) why CSB's often form first on the *conjugate* slip system, and what are the critical conditions; (ii) why MSB's often form first on the *conjugate* slip system, and what are the critical conditions; (iii) why and under what conditions do CSB's form

under multiple slip modes; (iv) how do we categorize CSB's and MSB's with respect to single slip shear bands and multiple slip shear bands.

It is very interesting to notice that elastic anisotropy can play an important role in determining the critical localization conditions, which means the elastic properties and plastic properties act together to determine the material's critical localization conditions. For example, for Cu or Ni_3Al single crystals, considering the elastic anisotropy may increase the critical hardening rate for localization 30% to 40%!

In this study, our latent hardening ratios q for multiple slip cases are all given as 1. For cases that $q < 1$ or $q > 1$, the results are in general the same as that $q = 1$ while h_{cr} may change 5–50% (no order of magnitude changes). What is important with reference to the value of the parameter q is that the latent hardening can substantially affect primary-conjugate slip activities. For example, with $q < 1$ the conjugate slip system can be activated long before the crystal reaches the symmetric boundary, while with $q > 1$ the conjugate slip system has to 'overshoot' the symmetric boundary in order to get activated, and there is a conjugate $\rightleftharpoons$ primary switch here. It is thus speculated that whether or not a shear band can form on planes that are close to the conjugate slip plane will be affected by latent hardening.

It is very important to understand that bifurcation analyses results can only serve as *necessary* conditions towards strain localization (see also Dao and Asaro, 1993), geometric factors like geometric softening or *geometric hardening*, different boundary conditions and latent hardening may play decisive roles in determining whether or not the shear bands develop and the orientation of the bands. Rigorously accounting for the non-uniform lattice rotations during the large deformation process is, therefore, very important. In order to achieve this and to obtain a more complete picture of localization process, we require large scale finite element calculations. In Part II of this series (Dao and Asaro, 1996a), we will specifically deal with non-uniform lattice rotations and study the deformation patterns of the different localization modes.

Acknowledgements

This work was supported by the National Science Foundation under contract number DMR91-10930. Partial support by the Office of Naval Research under contract number N0014-90-J1398 is also gratefully acknowledged. Computations were performed at the San Diego Supercomputer Center. The authors gratefully acknowledge helpful discussions with Dr. Ming Li and Dr. Owen Richmond.

References

Asaro, R.J. (1979), Geometrical effects in the inhomogeneous deformation of ductile single crystals, *Acta Metall.* 27, 445.

Asaro, R.J. (1983), Micromechanics of crystals and polycrystals, *Adv. Appl. Mech.* 23, 1.

Asaro, R.J. and J.R. Rice (1977), Strain localization in ductile single crystals, *J. Mech. Phys. Solids* 25, 309.

Bassani, J.L. (1994), Plastic Flow of Crystals, *Adv. Appl. Mech.* 30, 191.

Barendreght, J.A. and W.N. Sharpe, Jr. (1973), The effect of biaxial loading on the critical resolved shear stress of zinc single crystals, *J. Mech. Phys. Solids* 21, 113.

Beevers, C.J. and R.W. Honeycombe (1962), The deformation and fracture of aluminium–5.5% copper crystals, *Acta Metall.* 10, 17.

Chang, Y.W. (1979), An experimental study of shear localization in aluminium–copper single crystals, Ph.D. thesis, Brown University.

Chang, Y.W. and R.J. Asaro (1981), An experimental study of shear localization in aluminum–copper single crystals, *Acta Metall.* 29, 241.

Christoffersen, J., M.M. MMehrabadi and S. Nemat-Nasser (1981), A micromechanical description of granular material behavior, *J. Appl. Mech.* 48, 339.

Dao, M. and R.J. Asaro (1993), Non-Schmid effects and localized plastic flow in intermetallic alloys, *Mater. Sci. Eng. A* 170A, 1951.

Dao, M. and R.J. Asaro (1994), Coarse slip bands and the transition to macroscopic shear bands, *Scripta Metall.* 30, 791.

Dao, M. and R.J. Asaro (1996a), Localized deformation modes and non-Schmid effects in crystalline solids. Part II. Deformation patterns, this issue, Mech. Mater. 23 (1996) 103.

Dao, M. and R.J. Asaro (1996b), On the critical conditions of kink band formation in fiber composites with ductile matrix, *Scripta Metall.*, 34, 1771.

Dao, M., B.J. Lee and R.J. Asaro (1996), Non-Schmid effects on the behavior of polycrystals – with applications to Ni_3Al, *Metall. Trans. A* 27, 81.

Dève, H.E., S.V. Harren, C. McCullough and R.J. Asaro (1988), Micro and macroscopic aspects of shear band formation in internally nitrided single crystals of Fe–Ti–Mn alloys, *Acta Metall.* 36, 341.

Drucker, D.C. and M. Li (1993), Triaxial test instability of a nonassociated flow-rule model, *ASCE J. Eng. Mech.* 119, 1188.

Elam, C.F. (1927), Tensile tests on crystals – part IV. A copper alloy containing five percent aluminum, *Proc. R. Soc. A* 115A, 133.

Harren, S.V. and R.J. Asaro (1989), Nonuniform deformations in polycrystals and aspects of the validity of the Taylor model, *J. Mech. Phys. Solids* 37, 191.

Harren, S.V., H.E. Dève and R.J. Asaro (1988), Shear band formation in plane strain compression, *Acta Metall.* 36, 2435.

Heredia, F.E. and D.P. Pope (1989), Ductility and fracture behavior of single crystalline Ni_3Al with boron additions, in: ed. C.T. Liu, A.I. Taub, N.S. Stoloff and C.C. Koch, *High-Temperature Ordered Intermetallic Alloys III*, Materials Research Society, Pittsburg, PA, p. 287.

Hill, R. (1962), Acceleration waves in solids, *J. Mech. Phys. Solids* 10, 1.

Hill, R. and K.S. Havner (1982), Perspectives in the mechanics of elastoplastic crystals, *J. Mech. Phys. Solids* 30, 5.

Hill, R. and J.W. Hutchinson (1975), Bifurcation phenomena in the plane strain tension test, *J. Mech. Phys. Solids* 23, 239.

Hill, R. and J.R. Rice (1972), Constitutive analysis of elastic-plastic crystals at arbitrary strain, *J. Mech. Phys. Solids* 20, 401.

Inui, H., M.H. Oh, A. Nakamura and M. Yamaguchi (1992), Room-temperature tensile deformation of polysynthetically twinned (PST) crystals of TiAl, *Acta Metall.* 40, 3095.

Kawabata, T., T. Kanai and O. Izumi (1985), Positive temperature dependence of the yield stress in TiAl $L1_0$ type superlattice intermetallic compound single crystals at 293–1273 K, *Acta Metall.*, 33, 1355.

Kelly, A. and G.W. Groves (1970), *Crystallography and Crystal Defects*, Addison-Wesley, Reading, MA, p. 163.

Li, M. and D.C. Drucker (1994), Instability and bifurcation of a nonassociated extended Mises model in the hardening regime, *J. Mech. Phys. Solids* 42, 1883.

Mandel, J. (1947), Sur les lignes de glissement et le calcul des déplacements dans la déformation plastique, *C. R.* 225, 1272.

Mehrabadi, M.M. and S.C. Cowin (1978), Initial planar deformation of dilatant granular materials, *J. Mech. Phys. Solids* 26, 269.

Mehrabadi, M.M. and S.C. Cowin (1980), Prefailure and post-failure soil plasticity models, *ASCE J. Eng. Mech. Div.* 106, 991.

Minonishi, Y. (1991), Plastic deformation of single crystals of Ti_3Al with $D0_{19}$ structure, *Phil. Mag. A* 63, 1085.

Needleman, A. (1979), Non-normality and bifurcation in plane strain tension and compression, *J. Mech. Phys. Solids* 27, 231.

Nemat-Nasser, S. (1983), On finite plastic flow of crystalline solids and geomaterials, *J. Appl. Mech.* 50, 1114.

Nemat-Nasser, S., M.M. Mehrabadi and T. Iwakuma (1981), On certain macroscopic and microscopic aspects of plastic flow of ductile materials, in: ed. S. Nemat-Nasser, *Three-Dimensional Constitutive Relations and Ductile Fracture*, North-Holland Publishing Company, p. 157.

Paidar, V., D.P. Pope and V. Vitek, (1984), A theory of the anomalous yield behavior in $L1_2$ ordered alloys, *Acta Metall.* 32, 435.

Peirce, D., R.J. Asaro and A. Needleman (1982), An analysis of nonuniform and localized deformation in ductile single crystals, *Acta Metall.* 30, 1087.

Peirce, D., R.J. Asaro and A. Needleman (1983), Material rate dependence and localized deformation in crystalline solids, *Acta Metall.* 31, 1951.

Price, R.J. and A. Kelly (1964), Deformation of age-hardened aluminum alloy crystals – part II. fracture, *Acta Metall.* 12, 974.

Qin, Q. and J.L. Bassani (1992a), Non-Schmid yield behavior in single crystals, *J. Mech. Phys. Solids* 40, 813.

Qin, Q. and J.L. Bassani (1992b), Non-associated plastic flow in single crystals, *J. Mech. Phys. Solids* 40, 835.

Reid, C.N., A. Gilbert and G.T. Hahn (1966), Twinning slip and catastrophic flow in niobium, *Acta Metall.* 14, 975.

Rudnicki and Rice (1975), Conditions for the localization of deformation in pressure-sensitive dilatant materials, J. Mech. Phys. Solids 23, 371.

Spencer, A.J.M. (1964), A theory of the kinematics of ideal soils under plane strain conditions, *J. Mech. Phys. Solids* 12, 337.

Spitzig, W.A. (1981), Deformation behavior of nitrogenated Fe–Ti–Mn and Fe–Ti single crystals, *Acta Metall.* 29, 1359.

Spitzig, W.A., R.J. Sober and O. Richmond (1975), Pressure dependence of yielding and associated volume expansion in tempered martensite, *Acta Metall.* 23, 885.

Takasugi, T. and O. Izumi (1987), Plastic flow of Co_3Ti single crystals, *Acta Metall.* 35, 2015.

Takeuchi, S. and E. Kuramoto (1973), Temperature and orientation dependence of the yield stress in Ni_3Ga single crystals, *Acta Metall.* 21, 415.

Taylor, G.I. (1938), Analysis of plastic strain in a cubic crystal, in: ed. J.M. Lessels, *Stephen Timoshenko 60th Anniversary Volume*, Macmillan, New York, p. 218.

Vardoulakis, I., M. Goldscheider, and G. Gudehus (1978), Formation of shear bands in sand bodies as a bifurcation problem, *Int. J. Numer. Anal. Methods Geomech.* 2, 99.

Wasilewski, R.J., S.R. Butler and J.E. Hanlon (1967), Plastic deformation of single-crystal *NiAl*, *Trans. TMS-AIME* 239, 1357.

Yoo, M.H. (1987), Effects of elastic anisotropy on the anomalous yield behavior of cubic ordered alloys, in: ed. N.S. Stoloff, C.C. Koch, C.T. Liu and O. Izumi, *High-Temperature Ordered Intermetallic Alloys II*, Materials Research Society, Pittsburgh, PA, p. 207.